

# *Primeval galaxies*<sup>†</sup>

*Daniel Schaerer*

*Observatoire de Genève  
Université de Genève  
51, chemin des Maillettes  
CH-1290 Sauverny  
Switzerland*

*(daniel.schaerer@obs.unige.ch)*

and

*Observatoire Midi-Pyrénées  
Laboratoire d'Astrophysique, UMR 5572  
14 Avenue E. Belin  
F-31400 Toulouse, France*

<sup>†</sup> To appear in: "The emission line Universe", XVIII Canary Islands Winter School of Astrophysics, Ed. J. Cepa, Cambridge Univ. Press



# Contents

<b>1</b>	<b>Primeval galaxies</b>	<i>page</i> <b>2</b>
1.1	Introduction	2
1.2	PopIII stars and galaxies: a “top-down” theoretical approach	4
1.2.1	Primordial star formation	4
1.2.2	Primordial stars: properties	6
1.2.3	Primordial stars & galaxies: observable properties	7
1.2.4	Final fate	9
1.2.5	Nucleosynthesis & abundance pattern	10
1.2.6	Dust at high-z	10
1.3	Ly $\alpha$ physics and astrophysics	11
1.3.1	ISM emission and “escape”	11
1.3.2	Ly $\alpha$ : the observational problem	12
1.3.3	Lessons from local starbursts	14
1.3.4	Ly $\alpha$ radiation transfer	15
1.3.5	Lessons from Lyman Break Galaxies	19
1.3.6	Ly $\alpha$ trough the InterGalactic Medium	21
1.3.7	Ly $\alpha$ from sources prior to reionisation	22
1.3.8	Ly $\alpha$ Luminosity Function and reionisation	25
1.4	Distant/primeval galaxies: observations and main results	27
1.4.1	Search methods	27
1.4.2	Distant Ly $\alpha$ emitters	28
1.4.3	Lyman-break galaxies	33
1.4.4	What next?	40
	<i>References</i>	42

# 1

## *Primeval galaxies*

### 1.1 Introduction

What do we mean by primordial? According to the Webster dictionary “Primeval: adj. [primaevus, from: primus first + aevum age] of or relating to the earliest ages (as of the world or human history)”. In these lectures we will follow this definition and mostly discuss topics related to galaxies in the “early” universe, whose limit we somewhat arbitrarily define at redshifts  $z \gtrsim 6$ , corresponding approximately to the first billion years (Gyr) after the Big Bang. In contrast the frequently employed adjective “primordial”, defined as “Primordial: adj. [primordialis, from primordium origin, from primus first + ordiri to begin] a) first created or developed b) existing in or persisting from the beginning (as of a solar system or universe) c) earliest formed in the growth of an individual or organ”, should not be used synonymously, for obvious reasons. Luckily “primeval” encompasses more than “primordial”, otherwise there would not be much observational aspects to discuss (now in 2006-2007) in these lectures!

If we follow the history of discoveries of quasars and galaxies over the last few decades it is indeed impressive to see how progress has been made in detecting ever more distant objects, increasing samples at a given redshift, and in their analysis and interpretation. During the last decade, approximately since the pioneering observations of the Hubble Deep Field in 1996 (Williams et al. 1996) and the spectroscopic studies of a large sample of star forming galaxies at redshift 3 by Steidel and collaborators (Steidel et al. 1996), the observational limits have continuously been pushed further reaching now record redshifts of  $z \sim 7$  (secure, Iye et al. 2006) but maybe up to  $\sim 10$  (cf. Pelló et al. 2004, Richard et al. 2006, Stark et al. 2007).

Most of this progress has only been possible thanks to the Hubble Space Telescope, to the availability of 10m class telescopes (Keck, VLT, SUBARU), and to continuous improvements in detector technologies, especially in the optical and near-IR domain. Recently the IR Spitzer Space Telescope, with its 60cm mirror, has begun to play an important role in characterising the properties of the highest redshift galaxies.

Not only have observations progressed tremendously. Theory and numerical simulations now provide very powerful tools and great insight into the physics in the early Universe, first stars and galaxies. Within the model of hierarchical structure formation we have the following simplified global picture of primeval galaxies, their formation and interactions with the surrounding medium. Schematically, following the growth of quantum fluctuations after the Big Bang, one has in parallel: structure formation (hierarchical), star formation in sufficiently massive halos, “local” and “global” chemical evolution (including dust formation), and “local” and “global” reionisation †. These different processes are coupled via several feedback mechanisms (radiation, hydrodynamics). In this way the universe the first stars and galaxies are thought to form, to begin their evolution, to contribute to the chemical enrichment and dust production, and to gradually reionise the universe from shortly after the Big Bang to approximately 1 Gyr after that.

This global scenario and its various physical ingredients have been presented in depth in several excellent reviews to which the reader is referred to (Barkana & Loeb 2001, Bromm & Larson 2004, Ciardi & Ferrara 2005, Ferrara 2006). In these lectures I shall only briefly outline the most important theoretical aspects concerning the first stars and galaxies and their expected properties (Sect. 1.2). In Sect. 1.3 I will introduce and discuss Ly $\alpha$ , one of if not the strongest emission line in distant star forming galaxies, and review numerous results concerning this line and its use as a diagnostic tool. Finally I will present an overview of our current observational knowledge about distant galaxies, mostly Ly $\alpha$  emitters and Lyman break galaxies (Sect. 1.4). Open questions and some perspectives for the future are discussed in Sect. 1.4.4. It is the hope that these lectures may be helpful for students and other researchers in acquiring an overview of this very active and rapidly changing field, basics for its understanding, and maybe also provide some stimulations

† By *local* we here mean within a dark-matter (DM) halo, proto-cluster, or galaxies, i.e. at scales corresponding to the interstellar medium (ISM), intra-cluster medium (ICM), up to the “nearby” intergalactic medium (IGM). The *global* scale refers here to cosmic scales, i.e. scales of the IGM.

for persons working on related topics to explore the rich connections between different fields intertwined in the early universe and contributing to the richness of astrophysics.

## 1.2 PopIII stars and galaxies: a “top-down” theoretical approach

We shall now briefly summarise the expected theoretical properties governing the first generations of stars and galaxies, i.e. objects of primordial composition or very metal-poor.

### 1.2.1 Primordial star formation

In present-day gas, with a heavy element mass fraction (metallicity) up to  $\sim 2\%$ ,  $C^+$ , O, CO, and dust grains are excellent radiators (coolants) and the thermal equilibrium timescale is much shorter than the dynamical timescale. Hence large gas reservoirs can cool and collapse rapidly, leading to clouds with typical temperature of  $\sim 10$  K. In contrast, in primordial gas cloud would evolve almost adiabatically, since heavy elements are absent and H and He are poor radiators for  $T < 10^4$  K. However, molecules such as  $H_2$  or HD, can form and cool the gas in these conditions. Approximately, it is found that at metallicities  $Z \lesssim Z_{\text{crit}} = 10^{-5 \pm 1} Z_{\odot}$ , these molecules dominate the cooling (e.g. Schneider et al. 2002, 2004).

Starting from the largest scale relevant for star formation (SF) in galaxies, i.e. the scale of the DM halo, one can consider the conditions necessary for star formation (see e.g. Barkana & Loeb 2001, Ferrara 2007). Such estimates usually rely on timescale arguments. Most importantly, the necessary condition for fragmentation that the cooling timescale is shorter than the free-fall timescale,  $t_{\text{cool}} \ll t_{\text{ff}}$ , translates to a minimum mass  $M_{\text{crit}}$  of the DM halo for SF to occur as a function of redshift. A classical derivation of  $M_{\text{crit}}$  is found in Tegmark et al. (1997); typical values of  $M_{\text{crit}} \dagger$  are  $\sim 10^7$  to  $10^9 M_{\odot}$  from  $z \sim 20$  to 5. However, the value of  $M_{\text{crit}}$  is subject to uncertainties related to the precise cooling function and to the inclusion of other physical mechanisms (e.g. ultra-high energy cosmic rays), as discussed e.g. in the review of Ciardi & Ferrara (2005).

After SF has started within a DM halo, the “final products” may be

† Remember: This denotes the total DM mass, not the baryonic mass.

quite diverse, depending in particular strongly on a variety of radiative and mechanical feedback processes. Schematically, taking fragmentation and feedback into account, one may foresee the following classes of objects according to Ciardi et al. (2000): “normal” gaseous galaxies, naked star clusters (i.e. “proto-galaxies” which have blown away all their gas), and dark objects (where no stars formed, or where SF was rapidly turned off due negative radiative feedback). At very high redshift ( $z > 10$ ) naked star clusters may be more numerous than gaseous galaxies.

How does SF proceed within such a small “proto-galaxy” and what stars will be formed? Fragmentation may continue down to smaller scales. In general the mass of the resulting stars will depend on the fragment mass, the accretion rate, radiation pressure, and other effects such as rotation, outflows, competitive accretion etc., forming a rich physics which cannot be described here (see e.g. reviews by Bromm & Larson 2004, Ciardi & Ferrara 2005 and references therein) Most recent numerical simulations following early star formation at very low metallicities agree that at  $Z \lesssim Z_{\text{crit}}$  the smallest fragment are quite massive, and that they undergo a runaway collapse accompanied with a high accretion rate resulting in (very) massive stars (10–100  $M_{\odot}$  or larger), compared to a typical mass scale of  $\sim 1M_{\odot}$  at “normal” (higher) metallicities (cf. Bromm & Larson 2004). This suggests that the stellar initial mass function (IMF) may differ significantly from the present-day distribution at  $Z \lesssim Z_{\text{crit}} = 10^{-5 \pm 1} Z_{\odot}$ . The value of the critical metallicity is found to be determined mostly by fragmentation physics; in the transition regime around  $Z_{\text{crit}}$  the latter may in particular also depend on dust properties (cf. Schneider et al. 2002, 2004).

Determining the IMF at  $Z < Z_{\text{crit}}$  observationally is difficult and relies mostly on indirect constraints (see e.g. Schneider et al. 2006). The most direct approaches use the most metal poor Galactic halo stars found. From counts (metallicity distributions) of these stars Hernandez & Ferrara (2001) find indications for a increase of the characteristic stellar mass at very low  $Z$ . Similar results have been obtained by Tumlinson (2006), using also stellar abundance pattern. However, no signs of very massive ( $> 130 M_{\odot}$ ) stars giving rise to pair instability supernovae (see Sect. 1.2.4) have been found yet (cf. Tumlinson 2006). In Sect. 1.4 we will discuss attempts to detect PopIII stars and to constrain their IMF *in situ* in high redshift galaxies.

**1.2.2 Primordial stars: properties**

Now that we have formed individual (massive) stars at low metallicity, what are their internal and evolutionary properties? Basically these stars differ on two main points from their normal metallicity equivalents: the initial source of nuclear burning and the opacity in their outer parts. Indeed, since PopIII stars (or more precisely stars with metallicities  $Z \lesssim 10^{-9} = 10^{-7.3} Z_{\odot}$ ) cannot burn on the CNO cycle like normal massive stars, their energy production has to rely initially on the less efficient p-p chain. Therefore these stars have higher central temperatures. Under these conditions ( $T \gtrsim 10^{8.1}$  K) and after the build-up of some amount of He, the 3- $\alpha$  reaction becomes possible, leading to the production of some amounts of C. In this way the star can then “switch” to the more efficient CNO cycle for the rest of H-burning, and its structure (convective interior, radiative envelope) is then similar to “normal” massive stars. Given the high central temperature and the low opacity (dominated by electron scattering throughout the entire star due the lack of metals), these stars are more compact than their PopII and I correspondents. Their effective temperatures are therefore considerably higher, reaching up to  $\sim 10^5$  K for  $M \gtrsim 100 M_{\odot}$  (cf. Schaerer 2002). The lifetimes of PopIII stars are “normal” (i.e.  $\sim 3$  Myr at minimum), since  $L \sim M$ , i.e. since the luminosity increases approximately linearly with the increase of the fuel reservoir. Other properties of “canonical” PopIII stellar evolution models are discussed in detail in Marigo et al. (2001), Schaerer (2002), and references therein.

More sophisticated stellar evolution models including many physical processes related to stellar rotation are now being constructed (cf. Meynet et al. 2006, Ekström et al. 2006). Whereas before it was thought that mass loss would be negligible for PopIII and very metal-poor stars (since radiation pressure is very low and pulsational instabilities may only occur during a very short phase; cf. Kudritzki 2002, Baraffe et al. 2001), fast rotation – due to fast initial rotation and inefficient transport of angular momentum – may lead to mechanical mass loss, when these stars reach critical (break-up) velocity. Rotation also alters the detailed chemical yields, may lead to an evolution at hotter  $T_{\text{eff}}$ , even to WR stars, and it may alter final fate of PopIII/very metal-poor stars, which may in this way even avoid the “classical” pair instability supernova (PISN, cf. below). Many details and the implications of these models on observable properties of metal-free/very metal-poor populations still remain to be worked out.



## 1.2 PopIII stars and galaxies: a “top-down” theoretical approach 7

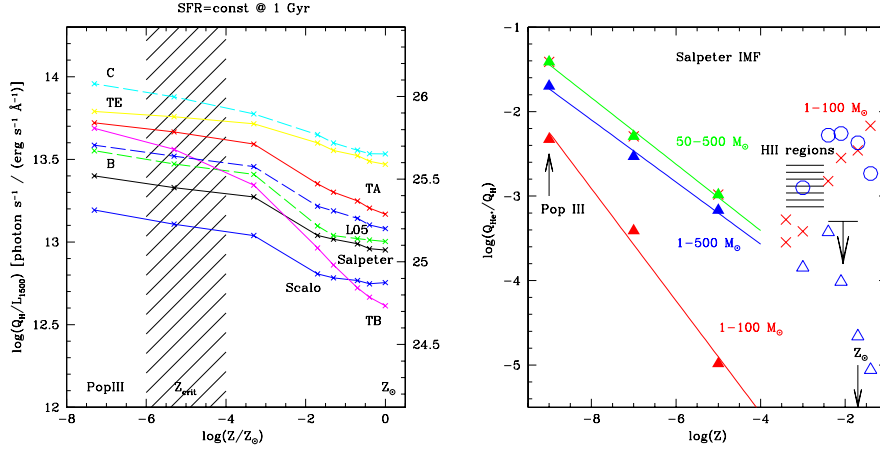


Fig. 1.1. **Left:** Relative output of hydrogen ionising photons to UV light, measured at 1500 Å restframe,  $Q_H/L_{1500}$ , as a function of metallicity for constant star formation over 1 Gyr. Results for different IMFs, including a Salpeter, Scalo and more top-heavy cases, are shown using different color codes. The shaded area indicates the critical metallicity range where the IMF is expected to change from a “normal” Salpeter-like regime to a more massive IMF. **Right:** Hardness  $Q(\text{He}^+)/Q(\text{H})$  of the  $\text{He}^+$  ionising flux for constant star formation as a function of metallicity (in mass fraction) and for different IMFs. At metallicities above  $Z \geq 4 \cdot 10^{-4}$  the predictions from our models (crosses), as well as those of Leitherer et al. (1999, open circles), and Smith et al. (2002, open triangles) are plotted. The shaded area and the upper limit (at higher  $Z$ ) indicates the range of the empirical hardness estimated from H II region observations. From Schaerer (2003)

### 1.2.3 Primordial stars & galaxies: observable properties

The observable properties of individual PopIII and metal-poor stars and of an integrated population of such stars can be predicted using stellar evolution models, appropriate non-LTE stellar atmospheres, and using evolutionary synthesis techniques (see e.g. Tumlinson et al. 2001, Bromm et al. 2001, and detailed discussions in Schaerer 2002, 2003).

Given the exceptionally high effective temperatures of PopIII stars on the zero age main sequence, such objects emit a larger fraction of the luminosity in the Lyman continuum and have a much harder ionising spectrum than higher metallicity stars. E.g. a PopIII star of  $5 M_\odot$  is still an ionising source! In other words, stellar populations at low metallicity are characterised by a high ionisation efficiency (per unit stellar mass formed) and by a hard spectrum, as illustrated in Figure 1.1. For an unchanged IMF, e.g. Salpeter, the ionising output normalised to the UV

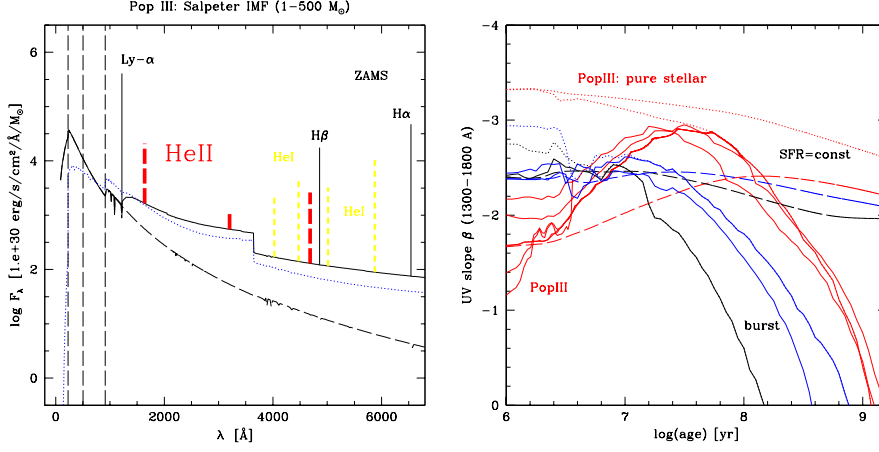


Fig. 1.2. **Left:** Spectral energy distribution of a very young PopIII galaxy including H and He recombination lines. The pure stellar continuum (neglecting nebular emission) is shown by the dashed line. For comparison the SED of the  $Z = 1/50Z_{\odot}$  population (model ZL: Salpeter IMF from 1 – 150  $M_{\odot}$ ) is shown by the dotted line. The vertical dashed lines indicate the ionisation potentials of H, He<sup>0</sup>, and He<sup>+</sup>. Note the presence of the unique He II features (shown as thick dashed lines) and the importance of nebular continuous emission. From Schaerer (2002). **Right:** Temporal evolution of the UV slope  $\beta$  measured between 1300 and 1800 Å from synthesis models of different metallicities and for instantaneous bursts (solid lines) and constant SF (long dashed lines). Black lines show solar metallicity models, red lines metallicities between  $Z = 10^{-5}$  and zero (PopIII), blue lines intermediate cases of  $Z = 0.004$  and  $0.0004$ . The dotted lines show  $\beta$  if nebular continuous emission is neglected, i.e. assuming pure stellar emission. Note especially the strong degeneracies of  $\beta$  in age and metallicity for bursts, the insensitivity of  $\beta$  on  $Z$  for constant SF, and the rather red slope for young very metal-poor bursts. From Schaerer & Pelló (2005).

flux density increases by a factor  $\sim 2$  or more from solar metallicity to PopIII. However, this increase may be much more substantial if the IMF favours massive stars at low  $Z$ , as argued before.

The predicted integrated spectrum of a very young (ZAMS) ensemble of PopIII stars is shown in Fig. 1.2. Its main characteristics are the presence of strong H emission lines (in particular strong Ly $\alpha$ , cf. below) due to the strong ionising flux, He<sup>+</sup> recombination lines (especially He II  $\lambda 1640$ ) due to spectral hardness, and strong/dominating nebular continuum emission (cf. Schaerer 2002). The strength of Ly $\alpha$  can be used to identify interesting PopIII or very-metal poor galaxy candidates (cf. Sect. 1.3). The detection of nebular He II  $\lambda 1640$  (if shown to be due to

stellar photoionisation, i.e. non-AGN origin) would be a very interesting signature of primordial (or very close to) stars. Indeed, as shown on the right of Fig. 1.1 very hard spectra are only predicted at  $Z \lesssim 10^{-5\dots-6} Z_{\odot}$ .

It is often heard that PopIII, primeval or similar galaxies should be distinguished by bluer colors, e.g. measured in the rest-frame UV, as one would naively expect. Although indeed the colors of stars get bluer on average with decreasing metallicity, this is not the case anymore for the integrated spectrum of such a population, since nebular continuum emission (originating from the H II regions surrounding the massive stars) may dominate the spectrum, even in the UV. This leads to a much redder spectrum, as shown in Fig. 1.2 (left). Taking this effect into account leads in fact to a non-monotonous behaviour of the slope (color) of the UV spectrum with metallicity, illustrated in Fig. 1.2 (right). This fact, and the dependence of the UV slope on the star formation history on timescales shorter than  $10^8$  to  $10^9$  yr, corresponding to 10-100 % of the Hubble time at  $z \gtrsim 6$ , show that the interpretation of the UV slope (or color) of primeval galaxies must be taken with great caution.

#### 1.2.4 Final fate

The end stages of very metal-poor and PopIII stars may also differ from those at higher metallicity, with several interesting consequences also for the observational properties of primeval galaxies. In particular such massive stars may at the end of their evolution show conditions in central temperature and density, such that the creation of electron-positron pairs occurs, leading to an instability which will completely disrupt the star. This phenomenon is known as pair instability supernova (PISN) †, and a rich literature exists about the phenomenon and many implications. Here we shall only summarise the main salient points and recent findings.

A recent overview of the different “final events” and remnants is found in Heger et al. (2003). PISN are thought to occur for stars with initial masses of  $M \sim 140\text{--}260 M_{\odot}$  a very low  $Z$ . Due to their high energy and to non-negligible time dilation which increases the duration of their “visibility”, PISN are potentially detectable out to very high redshift (see e.g. Weinmann & Lilly 2005, Scannapieco et al. 2005, Wise & Abel 2005). Large amounts of gas are ejected, as the event disrupts the star

† Sometimes the term pair creation SN or pair production SN is also used.

completely. Furthermore, the processed matter contains peculiar nucleosynthetic signatures which may in principle be distinguished from normal SN (cf. below). Finally PISN are also thought to be the first dust production factories in the universe (cf. Schneider et al. 2004). Thus PISN may be observable directly and indirectly, which would be very important to confirm or infirm the existence of such massive stars, i.e. to constrain the IMF of the first stellar generations. Currently, however, there is no such confirmation, as we will just discuss.

### ***1.2.5 Nucleosynthesis & abundance pattern***

Among the particularities of PISN are the production of large quantities of O and Si, which translate e.g. in large O/C and Si/C abundance ratios potentially measurable in the IGM. More generally one expects: roughly solar abundance of even nuclear charge nuclei (Si, S, Ar ...) and deficiencies in odd nuclei (Na, Al, P, V ...) i.e. a strong so-called odd/even effect, and no elements heavier than Zn, due to the lack of s- and r-processes (see Heger & Woosley 2002 for recent predictions).

Abundance studies of the most metal-poor halo stars in the Galaxy do not show the odd/even effect predicted for PISN. In face of our current knowledge, in particular on nucleosynthesis, quantitative analysis of the observed abundance pattern thus disfavour IMFs with a large fraction of stars with masses  $M \sim 140\text{--}260 M_{\odot}$  (Tumlinson 2006). However, the abundance pattern and other constraints are compatible with a qualitative change of the IMF at  $Z \lesssim 10^{-4} Z_{\odot}$  as suggested by simulations (cf. above).

### ***1.2.6 Dust at high- $z$***

Dust is known to be present out to the highest redshifts from damped Ly $\alpha$  absorbers (DLA), from sub-mm emission in  $z \sim 6$  Quasars (e.g. Walter et al. 2003), from a GRB host galaxy at  $z = 6.3$  (Stratta et al. 2007), and possibly also from the spectral energy distribution (SED) of some normal galaxies at  $z \sim 6$  (Schaerer & Pelló 2005). We also know that dust exists in the most metal-poor galaxies, as testified e.g. by the nearby galaxy SBS 0335-052 with a metallicity of  $\sim 1/50 Z_{\odot}$ .

Since the age of the universe at  $z > 6$  is  $\sim 1$  Gyr at most, longer-lived stars cannot be invoked to explain the dust production in primeval galaxies. Among the possible “short-lived” dust producers are SNII, PISN, maybe also Wolf-Rayet stars or massive AGB stars. SNII are known

dust producers (e.g. SN1987A), although maybe not producing enough dust. Efficient dust production is found in explosions of SNII and PISN (e.g. Todini & Ferrara 2001, Schneider et al. 2004). At zero metallicity PISN may provide a very very efficient mechanism, converting up to 7-20% of PISN mass into dust.

Evidence for dust produced by SN has been found from the peculiar extinction curve in the BAL QSO SDSS1048+46 at  $z = 6.2$ , which shows good agreement with SN dust models (Maiolino et al. 2004). Similar indications have been obtained recently from a GRB host galaxy at  $z \approx 6.3$  (Stratta et al. 2007). If this is a general feature remains, however, to be established. Furthermore the most important questions, including how common is dust in high- $z$  galaxies, in what quantities, up to which redshift, etc. have not yet been touched. Forthcoming IR to sub-mm facilities such as Herschel and especially ALMA will allow to address these important issues.

### 1.3 Ly $\alpha$ physics and astrophysics

As Ly $\alpha$ , one of the strongest emission lines in the UV, plays an important role in searches for and studies of distant and primeval galaxies, we wish to devote one lecture to this line, the basic principles governing it, its diagnostics and possible difficulties, empirical findings etc. To the best of my knowledge few if any reviews or lectures summarising these topics in a single text exist.

#### 1.3.1 ISM emission and “escape”

All ionised regions, i.e. H II regions, the diffuse ISM and alike regions in galaxies, emit numerous emission lines including recombination lines from H, He, and other atoms, and forbidden, semi-forbidden, and fine structure metal lines resulting from deexcitations of these atoms (see the textbooks of Osterbrock & Ferland 2006 or Dopita & Sutherland 2003, and Stasińska in these lecture notes). All galaxies with ongoing massive star formation (somewhat loosely called “starbursts” hereafter) emitting intense UV radiation and an ionising flux (i.e. energy at  $> 13.6$  eV) will thus “intrinsically”, viz. at least in their H II regions, show Ly $\alpha$  emission.

From quite simple considerations one can find that the luminosity in a given H recombination line is proportional to the number of ionising photons (i.e. Lyman-continuum photons),  $L(\text{Ly}\alpha, \text{H}\alpha, \dots) = c_l Q_H$ ,

where  $Q_H$  is the Lyman-continuum flux in photons  $s^{-1}$  and  $c_l$  a “constant” depending somewhat on the nebular temperature  $T_e$  and the electron density  $n_e$ . For hydrogen,  $\sim 2/3$  of the recombinations lead to the emission of a Ly $\alpha$  photon, corresponding to the transition from level 2 to the ground state (cf. Spitzer 1978, Osterbrock & Ferland 2006). Furthermore the relative intensities of two different H recombination lines are known and relatively slowly varying functions of temperature and density, e.g.  $I(\text{Ly}\alpha)/I(Hn) = c(T, n_e)$ .

Already in the sixties it was recognised that Ly $\alpha$  could be import for searches of primeval galaxies (e.g. Partidge & Peebles 1967). Indeed, at (very) low metallicities the Ly $\alpha$  line is expected to be strong if not dominant for several reasons: an increasing ionising flux from stellar populations, Ly $\alpha$  can become the dominant cooling line when few metals are present, an increased emissivity due to collisional excitation in a nebula with higher temperature. As a result up to  $\sim 10\%$  of the bolometric luminosity may be emitted in Ly $\alpha$ , rendering the line potentially detectable out to the highest redshifts! This prospect triggered various searches for distant Ly $\alpha$  emitters, which remained, however, basically unsuccessful until the 1990ies (see Sect. 1.4), for the reasons discussed below. In any case, it is interesting to note that most of the observational features predicted nowadays for PopIII galaxies (cf. Sect. 1.2.3) were anticipated by early calculations, such as Partridge & Peebles’ (1967), including of course the now famous Lyman-break (Sect. 1.4).

To anticipate it is useful to mention already here the basics of the Ly $\alpha$  escape problem. In short, for very low column densities of  $N_{HI} \gtrsim 10^{13} \text{ cm}^{-2}$  the Ly $\alpha$  line becomes already optically thick. Therefore radiation transfer within the galaxy determines the emergent line profile and the Ly $\alpha$  “transmission”! Furthermore, dust may destroy Ly $\alpha$  photons. Overall, the fate of Ly $\alpha$  photons emitted in a galaxy can be one of the following: 1) scattering until escape forming thus an extended Ly $\alpha$  “halo”; 2) destruction by dust; or 3) destruction through 2 photon emission. However, this process is only possible in the ionised region.

### ***1.3.2 Ly $\alpha$ : the observational problem***

As already mentioned, there were several unsuccessful searches for Ly $\alpha$  emission from  $z \sim 2-3$  “primordial” galaxies in the 1980-1990ies (cf. Pritchett 1994). Why these difficulties occurred could be understood by observations of nearby starbursts, which found one or two puzzles, namely a small number of Ly $\alpha$  emitting galaxies and/or lower than ex-

Fig. 1.3. **See Fig. 7 of Hayes et al. (2005) left out due to space limitations.** Observations of the nearby Blue Compact Galaxy ESO 338-IG04 from Hayes et al. (2005). **Left:** Ly $\alpha$  equivalent width map. Regions of high equivalent width show up in dark colours. Particularly visible are the diffuse emission regions outside the starburst region. Much local structure can be seen, particularly around knot A (the main UV knot) and the other bright continuum sources. **Right:** false colour image showing [OIII] in red, the UV continuum in green and the continuum subtracted Ly $\alpha$  image in blue.

pected Ly $\alpha$  emission. The second puzzle could of course in principle explain the first one. In particular UV spectra of nearby starbursts (Ly $\alpha$ ) taken with the IUE satellite and optical spectra (H $\alpha$ , H $\beta$ ) showed that: *i*) after extinction correction, the relative line intensity of e.g.  $I(\text{Ly}\alpha)/I(\text{H}\beta)$  was much smaller than the expected case B value and the Ly $\alpha$  equivalent width  $W(\text{Ly}\alpha)$  smaller than expected from evolutionary synthesis models, and *ii*) these findings do not depend on metallicity (e.g. Meier & Terlevich 1981, Hartmann et al. 1984, Deharveng et al. 1986, and other later papers).

Among the possible explanations put forward were: *a*) Dust which would destroy the Ly $\alpha$  photons (cf. Charlot & Fall 1993). *b*) An inhomogeneous ISM geometry, not dust, as a primarily determining factor (Giavalisco et al. 1996). *c*) A short “duty cycle” of SF to explain the small number of Ly $\alpha$  emitters. *d*) Valls-Gabaud (1993) argued that with an appropriate, i.e. metallicity-dependent, extinction law (i) was no problem. Also, he stressed the importance of underlying stellar Ly $\alpha$  absorption.

Rapidly dust as a sole explanation was ruled out by the observations of I Zw 18 and SBS 0335-052, the most metal-poor starbursts known, which show no Ly $\alpha$  emission, actually even a damped Ly $\alpha$  absorption profile (Kunth et al. 1994, Thuan & Izotov 1997). However, we now know (from ISO and Spitzer) that these objects contain also non-negligible amounts of dust (Thuan et al. 1999, Wu et al. 2007), although it is not clear if and how it is related to the line emitting regions, in particular spatially. From the absence of correlations between different measurements of extinction, Giavalisco et al. (1996) suggest that an inhomogeneous ISM geometry must be the primarily determining factor, not dust. However, no quantification of this effect was presented or proposed. More detailed observations of local starbursts have since provided new important pieces of information we will now briefly summarise.

**1.3.3 Lessons from local starbursts**

Indeed high-dispersion spectroscopy with HST has shown the presence of neutral gas outflows in 4 starbursts with Ly $\alpha$  in emission (P-Cygni profiles), whereas other starbursts with broad damped Ly $\alpha$  absorption do not show velocity shifts between the ionised emitting gas and the neutral ISM traced by O I or Si II (Kunth et al. 1998). The metallicities of these objects range from  $12 + \log(\text{O}/\text{H}) \sim 8.0$  to solar, their extinction is  $E_{B-V} \sim 0.1-0.55$ . From these observations Kunth et al. (1998) suggest that outflows and superwinds are the main determining factor for Ly $\alpha$  escape.

2-3 D studies of Ly $\alpha$  and related properties in nearby starbursts have been carried out with HST (UV) and integral field spectroscopy (optical) to analyse at *high spatial resolution* the distribution and properties of the relevant components determining Ly $\alpha$ , i.e. the young stellar populations, their UV slope (a measurement of the extinction), the ionised gas, and the resulting Ly $\alpha$  emission, absorption and the local line profile (e.g. Mas-Hesse et al. 2003, Kunth et al. 2003, Hayes et al. 2005). In ESO 338-IG04 (Tol 1914-416), for example, diffuse Ly $\alpha$  is observed corresponding to  $\sim 2/3$  of the total flux observed in large apertures (e.g. IUE), confirming thus the existence of a Ly $\alpha$  resonant scattering halo (Hayes et al. 2005). No clear spatial correlation between stellar ages and Ly $\alpha$  is found. However, correlations between the Ly $\alpha$  line kinematics and other kinematic tracers (NaID or H $\alpha$ ) are found.

Another interesting case is ESO 350-IG038, where Kunth et al. (2003) find two young star forming knots (B and C) with similar, high extinction, one showing Ly $\alpha$  emission the other not. Hence dust absorption cannot be the dominant mechanism here. Based on the observed H $\alpha$  velocity field, Kunth et al. suggests that kinematics is primarily responsible for the observed differences between the two regions.

A “unifying” scenario to explain the observed diversity of Ly $\alpha$  profiles in terms of an evolutionary sequence of starburst driven super-shells/superwind has been presented by Tenorio-Tagle et al. (1999) and confronted with local observations in the same paper and more in depth by Mas-Hesse et al. (2003).

In short we retain the following empirical results from nearby starbursts on Ly $\alpha$ :  $W(\text{Ly}\alpha)$  and Ly $\alpha/\text{H}\beta$  are often smaller than the case B prediction. No clear correlation of Ly $\alpha$  with metallicity, dust, and other parameters is found. Strong variations of Ly $\alpha$  are observed within a galaxy. A Ly $\alpha$  scattering “halo” is observed. Starbursts show com-



plex structure (super star clusters plus diffuse ISM), and outflows are ubiquitous. From the various observations it is clear that the formation of Ly $\alpha$  is affected by: 1) ISM kinematics, 2) ISM (HI) geometry, and 3) dust. However, the precise order of importance remains unclear and may well vary between different objects.

New, more complete high spatial resolution observations are needed. In parallel quantitative modeling including known constraints (stars, emitting gas, HI, dust plus kinematics) with 3D radiation transfer model remains to be done.

### 1.3.4 Ly $\alpha$ radiation transfer

#### 1.3.4.1 Basic line formation processes and examples

To gain insight on the physical processes affecting Ly $\alpha$ , to understand the variety of observed line profiles and their nature, and hence to develop quantitative diagnostics using Ly $\alpha$ , it is important to understand the basics of Ly $\alpha$  radiation radiation transfer. To do so we rely on the recent paper by Verhamme et al. (2006), where more details and numerous references to earlier papers can be found. Among recent papers shedding new light on Ly $\alpha$  radiation transfer we mention here the work of Hansen & Oh (2006) and Dijkstra et al. (2006ab).

The Ly $\alpha$  line optical depth can be written as

$$\tau_x(s) = 1.041 \times 10^{-13} T_4^{-1/2} N_H \frac{H(x, a)}{\sqrt{\pi}} \quad (1.1)$$

where  $T_4$  is the temperature in units of  $10^4$  K,  $N_H$  the neutral hydrogen column density, and  $H(x, a)$  the Hjerting function describing the Voigt absorption profile. Here  $x$  describes the frequency shift in Doppler units,  $x = \frac{\nu - \nu_0}{\Delta\nu_D} = -\frac{V}{b}$ , where the second equation gives the relation between  $x$  and a macroscopic velocity component  $V$  measured along the photon propagation (i.e. parallel to the light path and in the same direction).  $b$  is the usual Doppler parameter,  $b = \sqrt{V_{th}^2 + V_{turb}^2}$ . Eq. 1.1 shows that Ly $\alpha$  is very rapidly optically thick at line center, i.e. already for modest column densities ( $N_H > 3 \times 10^{13} \text{ cm}^{-2}$ ). For  $N_H = 10^{20}$  a very large number of scatterings ( $\sim 10^7$ ) are required to escape. However, velocity fields or a inhomogeneous medium can ease the escape (cf. below).

As true for other lines, the scattering of photons in the Ly $\alpha$  line is not a random walk: it corresponds to a walk in coupled spatial and frequency space, where transport is dominated by excursions to the line wings. In other words, photons propagate only over large distances

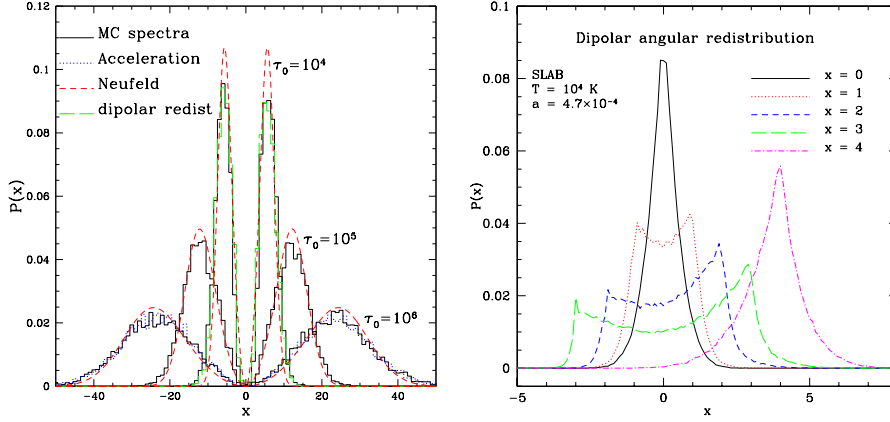


Fig. 1.4. **Left:** Predicted Ly $\alpha$  line profile for a monochromatic source embedded in a static medium with different  $N_{\text{H}}$  column densities. Note the characteristic symmetric double peak profile. The separation between the two peaks depends in particular on the total optical depth, i.e. on  $N_{\text{H}}$ . **Right:** Angle averaged frequency redistribution function for specific conditions ( $T$ , and Voigt-parameter  $a$ ). Shown is the probability distribution function for different input frequencies  $x = 0$  (line center) to 4 (“wing”). Figures from Verhamme et al. (2006).

allowing (long mean free path) them to escape when they are in the wings, where the opacity is lower. This already suffices to understand the formation of double peak Ly $\alpha$  line profiles in the case Ly $\alpha$  emission surrounded (or covered) by a static medium, as shown in Fig. 1.4 (left): all photons initially emitted at line centre (for illustration) are absorbed and “redistributed” to the wings, where they can escape. The higher the total optical depth, the larger the separation of the two peaks becomes. Asymmetries between the two peaks are of course introduced with shifts of the intrinsic emission frequency, or – equivalently – with an approaching/receding medium. These cases and many variations thereof are discussed in detail by Neufeld (1990).

In contrast to other scattering processes, Ly $\alpha$  scattering is neither coherent nor isotropic. The frequency redistribution, e.g. described by the angle averaged frequency redistribution functions  $R_{II}$  of Hummer (1962), is illustrated in Fig. 1.4 (right). Schematically, for input frequencies  $x_{\text{in}}$  close to the core the emergent photon has its frequency redistributed over the interval  $\sim [-x_{\text{in}}, +x_{\text{in}}]$ . Once photons are sufficiently far in wing they are re-emitted close to their input frequency, i.e.

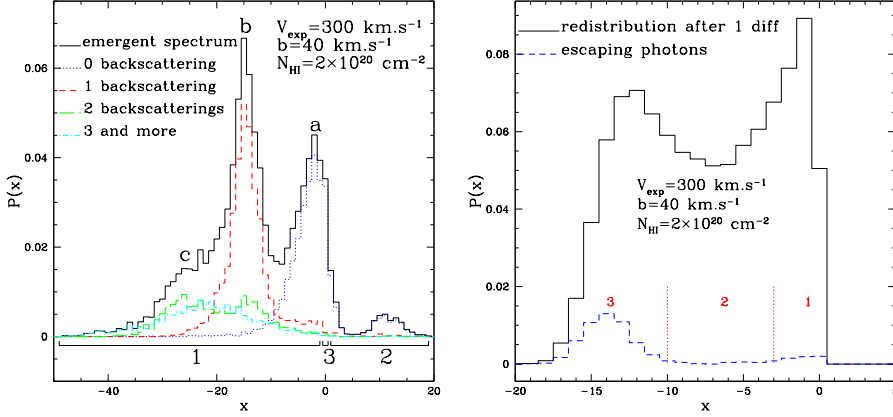


Fig. 1.5. **Left:** Emergent Ly $\alpha$  profile from an expanding shell with central monochromatic source. The different shapes can be described with the number of back-scatterings that photons undergo: bumps 1a and 2 are built-up with photons that did not undergo any backscattering, the highest peak located at  $x = -2v_{\text{exp}}/b$  (feature 1b) is composed of photons that undergo exactly one backscattering, and the red tail 1c is made of photons that undergo two or more backscatterings. See Verhamme et al. (2006) for more details. **Right:** Frequency distribution of the photons in the expanding shell after the first scattering. The black solid curve contains all photons, and the blue dotted one represents the histogram of photons which escaped after only one scattering. They form a bump around  $x \sim -2x(v_{\text{exp}})$ , which explains the appearance of feature 1b. See description in text. From Verhamme et al. (2006).

scattering is close to coherent in the comoving frame. This behaviour is fundamental to understand e.g. the formation of the emergent line profile for expanding shells, illustrated in Fig. 1.5. There detailed radiation transfer calculations show that the peak of the asymmetric Ly $\alpha$  profile is located approximately at the frequency Doppler-shifted by twice the expansion velocity resulting from photons from the backside of the shell (see Verhamme et al. 2006). This mostly results from two facts: first the reemission of the photons after their first scattering in the shell peaks at a Dopplershift of  $\sim 1 \times v_{\text{exp}}$  in the comoving reference frame of the shell, since the original Ly $\alpha$  photon emitted at line center ( $x = 0$ ) is seen in wing by the material in the shell (reemission close to coherence). In the external frame these photons have then frequencies between  $x \sim 0$  and  $-2x(v_{\text{exp}})$ . Now, the escape of the photons with the largest redshift being favoured, this will preferentially select photons from the back of the shell, creating thus a peak at  $-2x(v_{\text{exp}})$ . The interplay between

these different probabilities imprints the detailed line shape, discussed in more detail in Verhamme et al. (2006). For a given geometry, e.g. an expanding shell appropriate to model outflows in starbursts, a wide variety of Ly $\alpha$  profiles can be obtained depending on the shell velocity and its temperature, the column density, on the relative strength of the initial Ly $\alpha$  emission with respect to the continuum, and on the presence of dust (see Verhamme et al. 2006 for an overview). Let us now briefly discuss how dust affects the Ly $\alpha$  radiation transfer.

#### 1.3.4.2 Ly $\alpha$ transfer with dust

A simple comparison of the probability of Ly $\alpha$  photons to interact with dust,  $P_d = \frac{n_d \sigma_d}{n_H \sigma_H(x) + n_d \sigma_d}$ , shows that this event is quite unlikely, especially in the line core, where the Ly $\alpha$  cross section exceeds that of dust,  $\sigma_d$  by several orders of magnitudes. Despite this interactions with dust particles occur, especially in the wings, but also closer to line center since the overall probability for a photon to interact with dust is increased by the large number of line scattering occurring there. For this reason it is immediately clear that the dust destruction of Ly $\alpha$  photons depends also on the kinematics of the H I gas, where supposedly the dust is mixed in, although *per se* the interaction of UV photons with dust is independent of the gas kinematics.

The net result is a fairly efficient destruction of Ly $\alpha$  photons by dust, as e.g. illustrated for static cases by Neufeld (1990), and expanding shells by Verhamme et al. (2006). In the latter case the escape of Ly $\alpha$  photons is typically reduced by a factor  $\sim 2-4$  with respect to a simple reduction by  $\exp(-\tau_a)$ , where  $\tau_a$  is the dust absorption optical depth. Finally it is also interesting to note that dust does not only reduce the Ly $\alpha$  emission (or the line equivalent width), it also alters somewhat the line profile in a non-grey manner (cf. Ahn 2004, Hansen & Oh 2006), since its effect depends on Ly $\alpha$  scattering. See Verhamme et al. (2006) for illustrations.

#### 1.3.4.3 Ly $\alpha$ transfer: geometrical effects

Given the scattering nature of Ly $\alpha$  it is quite clear that the observed Ly $\alpha$  properties of galaxies depend also in particular on geometry. By this we mean the intrinsic geometry of the object, i.e. the spatial location of the “initial” Ly $\alpha$  emission in the H II gas, the distribution and kinematics of the scattering medium (namely the H I), but also the spatial region of this object which is ultimately observed. In other words the observed Ly $\alpha$  line properties (equivalent width and line profile) will in principle

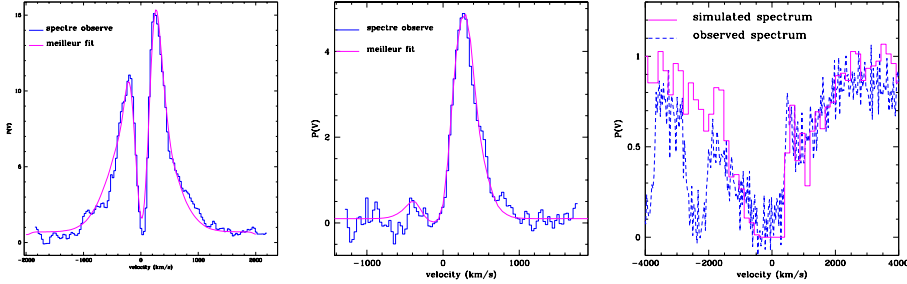


Fig. 1.6. Comparison of observed and modeled Ly $\alpha$  line profiles of  $z \sim 3$  LBGs showing a variety of different line profile morphologies, from double peaked, over P-Cygni, to broad absorption. See discussion in text. From Verhamme et al. (2007).

also vary if the observations provide an integrated spectrum of the entire galaxy or only a region thereof.

In an inhomogeneous ISM, UV continuum and Ly $\alpha$  line photons will also propagate in different ways, since their transmission/reflection properties differ. Such cases were e.g. discussed by Neufeld (1991) and Hansen & Oh (2006), who show that this can lead to higher Ly $\alpha$  equivalent widths.

In non-spherical cases, including for example galaxies with strong outflows and galactic winds with complex geometries and velocity structures one may of course also expect significant orientation effects on the observed Ly $\alpha$  line. Such cases remain largely to be explored in realistic 3D radiation transfer simulations.

### 1.3.5 Lessons from Lyman Break Galaxies

Having already discussed relatively nearby starburst galaxies, where spatial information is available, it is of interest to examine the empirical findings related to Ly $\alpha$  of more distant spatially unresolved objects, the so-called Lyman Break Galaxies (LBG) discussed also in more detail in Sect. 1.4 and by Giavalisco in this volume. These different categories of objects may help us understanding in particular Ly $\alpha$  emission and stellar populations in distant and primeval galaxies.

LBGs are galaxies with intense ongoing star formation, selected from their UV (restframe) emission. In 2003 approximately 1000 LBGs with spectroscopic redshifts were known, mostly studied by the group of Stei-

del (see Shapley et al. 2003). Since then the number has grown, but this study remains the most comprehensive one on  $z \sim 3$  LBGs. The restframe UV spectra of LBGs show stellar, interstellar and nebular lines testifying of the presence of massive stars. A diversity of Ly $\alpha$  line profiles, ranging from emission, over P-Cygni to broad absorption line profiles, and different strengths are observed. Interstellar (IS) lines are found blueshifted with respect to the stellar lines (defining the object redshift, when detected) by  $\Delta v(\text{abs} - \star) = -150 \pm 60 \text{ km s}^{-1}$ . A shift of  $\Delta v(\text{em} - \text{abs}) \sim 450\text{--}650 \text{ km s}^{-1}$  is also observed between the IS absorption lines and Ly $\alpha$ . Finally Shapley et al. (2003) find several correlations between the extinction,  $W(\text{Ly}\alpha)$ ,  $W(\text{IS})$ , and the star formation rate (SFR), which are not or poorly understood, at least until very recently (see Ferrara & Ricotti 2007 for a possible explanation).

From Ly $\alpha$  radiation transfer modeling discussed before, the observed shifts between stellar, IS lines and Ly $\alpha$  are naturally understood if the geometry is that of a “global” expanding shell (Verhamme et al. 2006). The IS lines are then formed by absorption of the UV continuum light from a central starburst in the shell along the line of sight towards the observer. Their blueshift with respect to the stars measures thus the expansion velocity  $v_{\text{exp}}$ . One then obtains naturally  $\Delta v(\text{em} - \text{abs}) \sim 3 \times |\Delta v(\text{abs} - \star)| = 3v_{\text{exp}}$ , since Ly $\alpha$  originates from the back of shell redshifted by  $2v_{\text{exp}}$ . This result indicates that large-scale, fairly symmetric shell structures must be a good description of the outflows in LBGs.

What causes the variety of observed Ly $\alpha$  line profiles and what does this tell us about these galaxies? Using the radiation transfer code described in Verhamme et al. (2006) we have recently undertaken the first detailed modeling of typical LBGs at  $z \sim 3$ , in particular objects from the FORS Deep Field observed by Tapken et al. (2007) at a spectral resolution  $R \sim 2000$ , sufficient to do detailed line profile fitting. Assuming the spherically expanding shell model motivated in particular by the correct velocity shifts just mentioned, the full variety of profiles can be reproduced for the observed values of  $v_{\text{exp}}$  and extinction, and by varying  $N_{\text{H}}$ , and intrinsic Ly $\alpha$  line parameters ( $W$  and FWHM).

Three such examples are illustrated in Fig. 1.6. Fitting the double peak profile of FDF 4691 (left), is only possible with low velocities, i.e. conditions close to a static medium (cf. Fig. 1.4). Such Ly $\alpha$  profiles are relatively rare; other cases with such double peak profiles include the Ly $\alpha$  blob observed by Wilman et al. (2005) and interpreted by them as a “stalled” expanding shell, or even as a collapsing protogalaxy (Dijk-

stra et al. 2006b). The profile of FDF 4454 (middle), quite typical of LBGs, indicates a typical expansion velocity of  $v_{\text{exp}} \sim 220 \text{ km s}^{-1}$  and a low extinction, compatible with its very blue UV slope. Finally, the profile of the lensed galaxy cB58 (right) from Pettini et al. (2000) is well reproduced with the observed expansion velocity and extinction ( $v_{\text{exp}} \sim 255 \text{ km s}^{-1}$ ,  $E_{B-V} = 0.3$ ). The fits yield in particular constraints on the column density  $N_{\text{H}}$  and the intrinsic Ly $\alpha$  line parameters ( $W$  and FWHM). This allows us to examine the use of Ly $\alpha$  as a SFR indicator, to provide constraints on the SF history and age of these galaxies, and to shed new light on the observed correlations between Ly $\alpha$  and other properties of LBGs (see Verhamme et al. 2007). Understanding Ly $\alpha$  in galaxies for which sufficient observations are available and located at different redshift is of great interest also to learn how to exploit the more limited information available for objects at higher  $z$ , including primeval galaxies (see Section 1.4).

### 1.3.6 Ly $\alpha$ trough the InterGalactic Medium

Having discussed the properties of Ly $\alpha$  line formation and radiation transfer effects in galaxies, we will now examine how the Ly $\alpha$  profile is transformed/transmitted on its way to the observer, i.e. through the intergalactic medium (IGM).

In this situation we consider radiation from a distant background source passing through one or several ‘‘H I clouds’’. This geometry leads to a very simple case where Ly $\alpha$  photons are absorbed and then either scattered out of the line of sight or absorbed internally by dust. In other words *no true radiation transfer needs to be computed*, and the resulting Ly $\alpha$  profile of the radiation emerging from the cloud is simply the input flux attenuated by a Voigt absorption profile characteristic of the cloud properties. For a given density and (radial) velocity – or equivalently redshift – distribution along the line of sight, the computation of the total attenuation and hence of the observed spectrum is thus straightforward.

The observational consequences for a distant source will thus be: 1) the imprint of a number of (discrete) absorption components on top of the background source spectrum due to intervening H I clouds or filaments, and 2) an alteration of the emergent galactic Ly $\alpha$  profile plus a reduction of the Ly $\alpha$  flux if neutral H is present close in velocity/redshift space to the source. The first is well known observationally as the Ly $\alpha$  forest, leading even to a complete absorption (the so-called

Gunn-Peterson trough) in distant ( $z \sim 6$ ) quasars (see the review by Fan et al. 2006). The appearance of a complete Gunn-Peterson trough in high- $z$  quasars implies a quantitative change of the ionisation of the IGM, possibly tracing the end of the epoch of cosmic reionisation (cf. Fan et al. 2006). The second effect leads e.g. to the alteration of the Ly $\alpha$  profile and to a strong reduction of the Ly $\alpha$  flux in high- $z$  quasar, due to absorption by the red damping wing of Ly $\alpha$  by nearby H I (cf. Miralda-Escudé 1998, and observations by Fan et al. 2003).

The two effects just discussed have the following immediate implications:

- The SED of high- $z$  galaxies is altered by Lyman-forest attenuation at wavelengths shorter than Ly $\alpha$  ( $< 1216 \text{ \AA}$ ). A statistical description of this attenuation is given by Madau (1995).
- For  $z \gtrsim 4$ –5 the Lyman-forest attenuation is so strong that it effectively leads to a spectral break at Ly $\alpha$ , replacing therefore the “classical” Lyman-break (at  $912 \text{ \AA}$ ) due to photoelectric absorption by H I). The Ly $\alpha$ -break becomes then the determining feature for photometric redshift estimates.
- The reduction of the Ly $\alpha$  flux implies that *a*) determinations of the SFR from this line will underestimate the true SFR, *b*) the observed Ly $\alpha$ -luminosity function (LF) does not correspond to the true (intrinsic) one, and *c*) the detectability of high- $z$  Ly $\alpha$  emitters (hereafter LAE) is reduced.
- The Ly $\alpha$  profile, Ly $\alpha$  transmission, and the Ly $\alpha$  luminosity function contain information on the ionisation fraction of hydrogen and can hence in principle constrain cosmic reionisation.

We will now discuss how/if it is still possible to observe LAE beyond the reionisation redshift.

### ***1.3.7 Ly $\alpha$ from sources prior to reionisation***

How is it possible to observe Ly $\alpha$  emission from sources “beyond the end of reionisation”, i.e. at very high redshift where the IGM contains a significant fraction of neutral hydrogen which absorbs the Ly $\alpha$  emission? The way to achieve this is in principle quite simple and sketched in Fig. 1.7. It suffices to create around the Ly $\alpha$  source a “cosmological” H II region big enough so that no or very little H I is present at velocities – i.e. redshifts – close to the source. In this way the attenuation close to the Ly $\alpha$  emission is avoided and the line flux from this distant source can



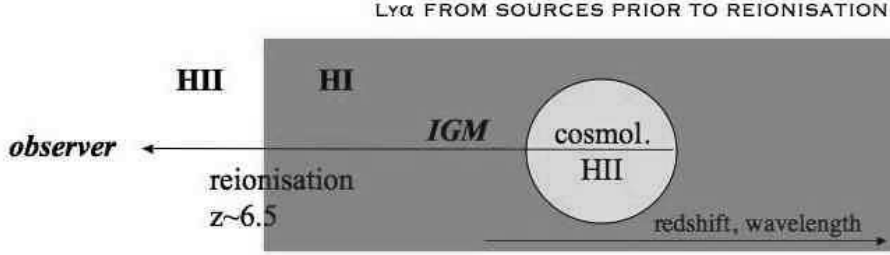


Fig. 1.7. Schematic representation of a star forming galaxy situated beyond the reionisation redshift (here indicated at  $z_r \sim 6.5$ ), its surrounding cosmological H II region, the neutral IGM down to  $z_r$ , and the transparent (ionised) IGM towards the observer. Redshift and the observed Ly $\alpha$  wavelength increase to the right.

propagate freely to the observer, since it comes from the most redshifted part along the line of sight.

So, how are these cosmological H II regions created? Obviously this requires one or several sources (galaxies or quasars) producing ionising photons which are able to escape the galaxy and can then progressively ionise the surrounding IGM. This is referred to as the “proximity effect”. The properties and the evolution of cosmological H II regions have been studied and described analytically in several papers (see e.g. Shapiro & Giroux 1987, Cen & Haiman 2000, and review by Barkana & Loeb 2001). For example, neglecting recombinations in the IGM (since for the low IGM densities the recombination timescale is much longer than the Hubble time) and assuming that the ionising source is “turned on” and constant during the time  $t_Q$  the Stroemgren radius (size) of the H II region becomes

$$R_{t_Q} = \left[ \frac{3\dot{N}_{ph}t_Q}{4\pi \langle n_H \rangle} \right]^{1/3}, \quad (1.2)$$

where  $\dot{N}_{ph} = f_{esc}Q_H$  is escaping ionising flux and  $\langle n_H \rangle$  the mean IGM density taking possibly a non-uniform density distribution into account. The residual H I fraction inside the H II region is given by photoionisation equilibrium and can also be computed. Then the resulting attenuation  $e^{-\tau}$  can be computed by integrating the optical depth along the line of sight

$$\tau(\lambda_{obs}, z_s) = \int_{z_r}^{z_s} dz c \frac{dt}{dz} n_H(z) \sigma_\alpha(\lambda_{obs}/(1+z)). \quad (1.3)$$

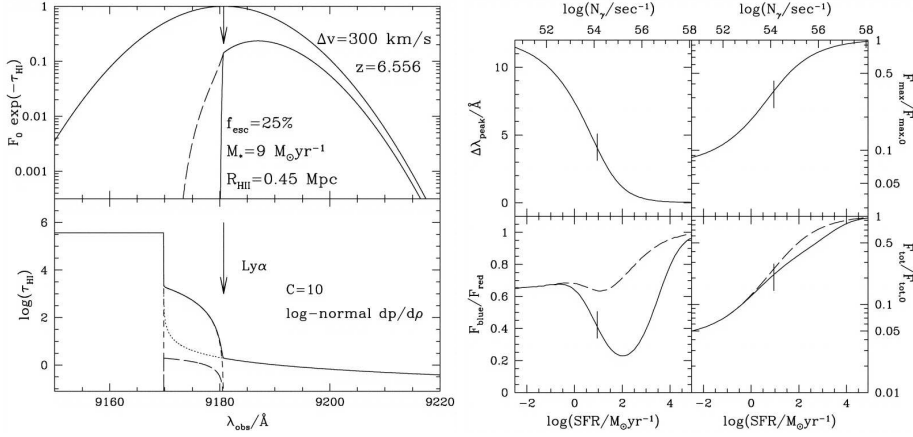


Fig. 1.8. Predicted Ly $\alpha$  line profile, Ly $\alpha$  transmission and other properties from the model of a  $z = 6.56$  lensed galaxy taking IGM absorption into account. from Haiman (2002). **Left:** Intrinsic and resulting line profile (top), opacities leading to the Ly $\alpha$  attenuation. **Right:** Parameters, such as asymmetry, peak position, and total transmission (bottom right) of the predicted Ly $\alpha$  line as a function of the SFR.

Here  $z_s$  is the source redshift,  $z_r$  a limiting redshift (the redshift of reionisation in Fig. 1.7) below which the IGM is supposed to be transparent, and  $\sigma_\alpha$  is the Ly $\alpha$  absorption cross section.

For example, the observability of Ly $\alpha$  from a  $z = 6.56$  galaxy observed by Hu et al. (2002) has been examined with such a model by Haiman (2002). The results are illustrated in Fig. 1.8. For a source with  $SFR = 9 M_\odot \text{ yr}^{-1}$ , an age of  $\sim 100$  Myr, and an escape fraction  $f_{esc} = 25\%$  the proper (comoving) radius of the H II region is approximately 0.45 (3) Mpc. Assuming an intrinsic Ly $\alpha$  profile with a width of  $FWHM = 300 \text{ km s}^{-1}$  Haiman obtains a transmission of  $\sim 16\%$  of the Ly $\alpha$  flux and an asymmetric line profile, as observed. A wider range of transmission encompassing also this value is found from an independent estimate based on stellar population modeling (cf. Schaerer & Pelló 2005).

In the picture described above, the Ly $\alpha$  transmission is expected to increase with increasing  $SFR$ , escape fraction, source lifetime, and intrinsic line width, as also shown in Fig. 1.8 (right). The first three increase the size of the cosmological H II region; with the latter a higher fraction of the line flux is emitted far from line center reducing thus the absorption by the red damping wing in the H I. Other factors also affect the Ly $\alpha$  transmission and the resulting line profile: IGM infall,

outflows (galactic winds), peculiar velocities of the emitting gas within halo, the halo mass etc. See Haiman (2002) and Santos (2004), which have examined these effects.

In a more realistic setting several “complications” can occur to this simple model (see e.g. Gnedin & Prada 2004, Furlanetto et al. 2004, Wyithe & Loeb 2004).

- Clustering of sources helps to create a larger H II region. Since the clustering probability increases with  $z$  and for fainter galaxies, this could play an important role for the detectability of high redshift Ly $\alpha$  sources.
- In a non-homogeneous structure around the source the H II regions are expected to deviate from spherical symmetry, since the ionisation fronts will propagate more rapidly into directions with a lower IGM density.

From this it is clear that strong variations depending on the object, its surroundings, and the viewing direction are expected and the simple scaling properties of the spherical models described before may not apply. A statistical approach using hydrodynamic simulations will be needed.

In short, the answer to the question “Is Ly $\alpha$  emission from sources prior to reionisation detectable?” is affirmative from the theoretical point of view, but the transmission depends on many factors! In any case, searches for such objects are ongoing (cf. Sect. 1.4.2) and will provide the definite answer.

### ***1.3.8 Ly $\alpha$ Luminosity Function and reionisation***

As a last illustration of the use of Ly $\alpha$  in distant, primeval galaxies we shall now briefly discuss the statistics of LAE, in particular the Ly $\alpha$  luminosity function LF(Ly $\alpha$ ), how it may be used to infer the ionisation fraction of the IGM at different redshift, and difficulties affecting such approaches.

Since, as discussed above, the presence of neutral hydrogen in the IGM can reduce the Ly $\alpha$  flux of galaxies, it is clear that the Ly $\alpha$  LF is sensitive to the ionisation fraction  $x_{HI}$ . If we knew the intrinsic LF( $z$ ) of galaxies at each redshift, a deviation of the observed LF from this intrinsic distribution could be attributed to attenuation by H I, and hence be used to infer  $x_{HI}$  (cf. Fig. 1.9). In practice the approach is of course to proceed to a differential comparison of LF(Ly $\alpha$ ) with redshift.

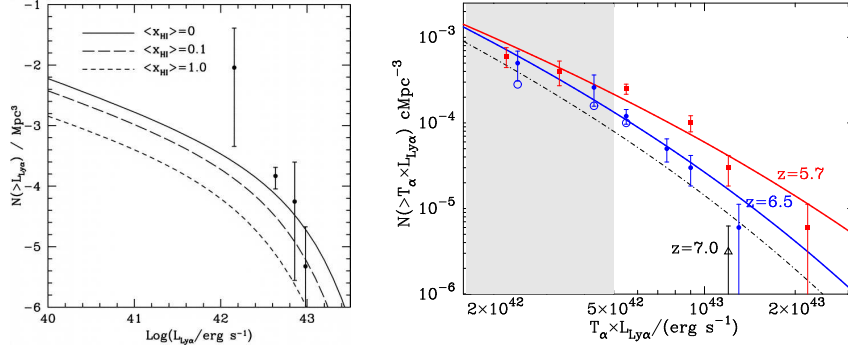


Fig. 1.9. **Left:** predicted Ly $\alpha$  LFs for a fully ionised IGM (no attenuation case, i.e. the  $z = 5.7$  LF; solid curve), and for an IGM with an increasing neutral H fraction  $x_{HI}$ . From Haiman & Cen (2005). **Right:** Predicted and observed Ly $\alpha$  LF at  $z = 5.7$  and  $6.5$ . The LF model is that by Dijkstra et al. (2006c). According to these authors the observed ecline of the Ly $\alpha$  LF attributed to the evolution of the halo mass function hosting the Ly $\alpha$  emitters.

Indeed, from simple Ly $\alpha$  attenuation models like the ones described in the previous section, a rapid decline of the LF is expected when approaching the end of reionisation.

Haiman & Spaans (1999) were among the first to advocate the use of LF(Ly $\alpha$ ) and to make model predictions. Since then, and after the detection of numerous LAEs allowing the measurement of the Ly $\alpha$  LF out to redshift  $z = 6.5$  (cf. Section 1.4.2), several groups have made new predictions of the Ly $\alpha$  LF and have used it to constrain cosmic reionisation. Some prominent examples are Malhotra & Rhoads (2004), Le Delliou et al. (2005, 2006), and Furlanetto et al. (2006).

One of the most recent of such attempts is presented by Dijkstra et al. (2006c) who predict the Ly $\alpha$  LF based on a modified Press-Schechter formalism and introducing two main free parameters, a star formation duty-cycle  $\epsilon_{DC}$  and another parameter depending on the SF efficiency, the escape fraction and the Ly $\alpha$  transmission of the IGM. They find a typical IGM transmission of  $T_{\alpha} \sim 30\%$  at  $z = 5.7$ . Adjusting the observed LFs at  $z = 5.7$  and  $6.5$  (where Quasars already indicate a significant change of the ionisation fraction  $x_{HI}$  as discussed in Sect. 1.3.6) Dijkstra et al. (2006c) find good fits without the need for a strong change of the ionisation state advocated in other studies (see Fig. 1.9) The observed decline of the Ly $\alpha$  LF between  $z = 5.7$  and  $6$  is attributed to the evolution of the halo mass function hosting the Ly $\alpha$  emitters. In this case this may translate to a lower limit of  $\sim 80\%$  for the frac-

tion of ionised H at  $z = 6.5$ . This serves to illustrate the potential of LF(Ly $\alpha$ ) analysis, but also the potential difficulties and the room for improvements.

Finally let us also note that Hu et al. (2005) do not find an evolution of the mean Ly $\alpha$  line profile between  $z = 5.7$  and  $6.5$ , in agreement with the above conclusion.

#### 1.4 Distant/primeval galaxies: observations and main results

Before we discuss searches for distant galaxies, provide an overview of the main results, and discuss briefly open questions we shall summarise the basic observational techniques used to identify high redshift galaxies.

##### 1.4.1 Search methods

The main search techniques for high- $z$  galaxies can be classified in the two following categories.

- (i) The Lyman break or drop-out technique, which selects galaxies over a certain redshift interval by measuring the Lyman break, which is the drop of the galaxy flux in the Lyman continuum (at  $\lambda < 912 \text{ \AA}$ ) of the Ly $\alpha$  break (shortward of Ly $\alpha$ ) for  $z \gtrsim 4$ – $5$  galaxies (cf. above). This method requires the detection of the galaxy in several (sometimes only 2, but generally more) broad-band filters.
- (ii) Emission line searches (targeting Ly $\alpha$  or other emission lines). Basically three different techniques may be used: 1) Narrow Band (NB) imaging (2D) e.g. of a wide field selecting a specific redshift interval with the transmission of the NB filter. Long slit spectroscopy (1D) for “blind searches” e.g. along critical line in lensing clusters, or observations with Integral Field Units (3D) allowing to explore all three spatial directions (2D imaging + redshift). The first one is currently the most used technique.

In practice, and to increase the reliability, several methods are often combined.

Surveys/searches are being carried out in blank fields or targeting deliberately gravitational lensing clusters allowing one to benefit from gravitational magnification from the foreground galaxy cluster. For galaxies at  $z \lesssim 7$  the Lyman-break and Ly $\alpha$  is found in the optical domain. Near-IR ( $\gtrsim 1 \mu\text{m}$ ) observations are necessary to locate  $z \gtrsim 7$  galaxies.

The status in 1999 of search techniques for distant galaxies has been summarised by Stern & Spinrad (1999). For more details on searches and galaxy surveys see the lecture notes of Giavalisco (these proceedings).

#### 1.4.2 Distant Ly $\alpha$ emitters

Most of the distant known Ly $\alpha$  emitters (LAE) have been found through narrow-band imaging with the SUBARU telescope, thanks to its wide field imaging capabilities.  $z \sim 6.5$ – $6.6$  LAE candidates are e.g. selected combining the three following criteria: an excess in a narrowband filter (NB921) with respect to the continuum flux estimated from the broad  $z'$  filter, a  $5\sigma$  detection in this NB filter, and an  $i$ -dropout criterium (e.g.  $i - z' > 1.3$ ) making sure that these objects show a Ly $\alpha$ break. Until recently 58 such LAE candidates were found, with 17 of them confirmed subsequently by spectroscopy (Taniguchi et al. 2005, Kashikawa et al. 2006). The Hawaii group has found approximately 14 LAE at  $z \sim 6.5$  (Hu et al. 2005, Hu & Cowie 2006). The current record-holder as the most distant galaxy with a spectroscopically confirmed redshift of  $z = 6.96$  is by Iye et al. (2006). Six candidate Ly $\alpha$  emitters between  $z = 8.7$  and  $10.2$  were recently proposed by Stark et al. (2007) using blind long-slit observations along the critical lines in lensing clusters.

LAE have for example been used with SUBARU to trace large scale structure at  $z = 5.7$  thanks to the large field of view (Ouchi et al. 2005).

Overall, quite little is known about the properties of NB selected LAE, their nature and their relation to other galaxy types (LBG and others, but cf. Sect. 1.4.3), since most of them – especially the most distant ones – are detected in very few bands, i.e. their SEDs is poorly constrained. The morphology of the highest- $z$  LAEs is generally compact, indicating ionised gas with spatial extension of  $\sim 2$ – $4$  kpc or less (e.g. Taniguchi et al. 2005, Pirzkal et al. 2006).

Although showing SF rates (SFR) of typically 2 to  $50 M_{\odot} \text{ yr}^{-1}$ , the SFR density of LAE is only a fraction of that of LBGs at all redshifts. For example at  $z \sim 5$ – $6.5$ , Taniguchi et al. (2005) estimate the star formation rate density (SFRD) from Ly $\alpha$  emitters as  $\text{SFRD(LAE)} \sim 0.01 \times \text{SFRD(LBG)}$ , or up to 10 % of  $\text{SFRD(LBG)}$  at best if allowing for LF corrections. At the highest  $z$  this value could be typically  $3 \times$  higher if the IGM transmission of  $\sim 30\%$  estimated by Dijkstra et al. (2006c) applies. Shimasaku et al. (2006) have found a similar space density or UV LF for LAE and LBG at  $z \sim 6$ , and argue that LAEs contribute at least 30 % of the SFR density at this redshift.

The typical masses of LAE are still uncertain and being debated. For example, Lai et al. (2007) find stellar masses of  $M_{\star} \sim 10^9$  and  $10^{10} M_{\odot}$  for three LAE at  $z \sim 5.7$ , whereas Prizkal et al. (2006) find much lower values of  $M_{\star} \sim 10^6$  and  $10^8 M_{\odot}$  for their sample of  $z \sim 5$  Ly $\alpha$  galaxies. Finkelstein et al. (2006) find masses between the two ranges for  $z \sim 4.5$  LAEs. Selection criteria may explain some of these differences; e.g. the Lai et al. objects were selected for their detection at 3.6 and 4.5  $\mu\text{m}$  with Spitzer. Mao et al. (2006) argue that LAEs are limited to a relatively narrow mass range around  $M_{\star} \sim 10^9 M_{\odot}$ . Further studies will be necessary to properly understand the connections between LBG and LAE and the evolution of the two populations with redshift.

#### 1.4.2.1 PopIII signatures in LAE?

The Large Area Lyman- $\alpha$  (LALA) survey by Rhoads and collaborators, carried out on 4m class telescopes, has been one of the first to find a significant number of LAE at high redshift ( $z = 4.5, 5.7$ , and later also objects at 6.5). Among the most interesting results found from LALA is the finding of a large fraction of LAE with an apparently high median Ly $\alpha$  equivalent width, compared to expectations from normal stellar populations (see Fig. 1.10). Indeed, half of their  $z = 4.5$  candidates show  $W(\text{Ly}\alpha)$  in excess of  $\sim 200\text{--}300 \text{ \AA}$  (Malhotra & Rhoads 2002), a value expected only for very young starbursts, populations with extreme IMFs, or very metal-poor (or PopIII) stars (cf. Schaerer 2003). Malhotra & Rhoads (2002) suggested that these could be AGN or objects with peculiar top-heavy IMFs and/or PopIII dominated. In this context, and to explain other observations, Jimenez & Haiman (2006) also advocate a significant fraction of PopIII stars, even in  $z \sim 3\text{--}4$  galaxies. Recently Hansen & Oh (2006), reviving an idea of Neufeld (1991), have suggested that the observed  $W(\text{Ly}\alpha)$  could be “boosted” by radiation transfer effects in a clumpy ISM.

Follow-up observations of the LALA sources have allowed to exclude the narrow-line AGN “option” (Wang et al. 2004), but have failed to provide further explanations of this puzzling behaviour. A fraction of  $\sim 70\%$  of the LALA LAE have been confirmed spectroscopically; some high equivalent widths measurement could also be confirmed spectroscopically †. Deep spectroscopy aimed at detecting other emission lines, including the He II  $\lambda 1640$  line indicative of a PopIII contribution (cf. Sect. 1.2.3), have been unsuccessful (Dawson et al. 2004), although the

† But aperture effects may still lead to an overestimate of  $W(\text{Ly}\alpha)$ .

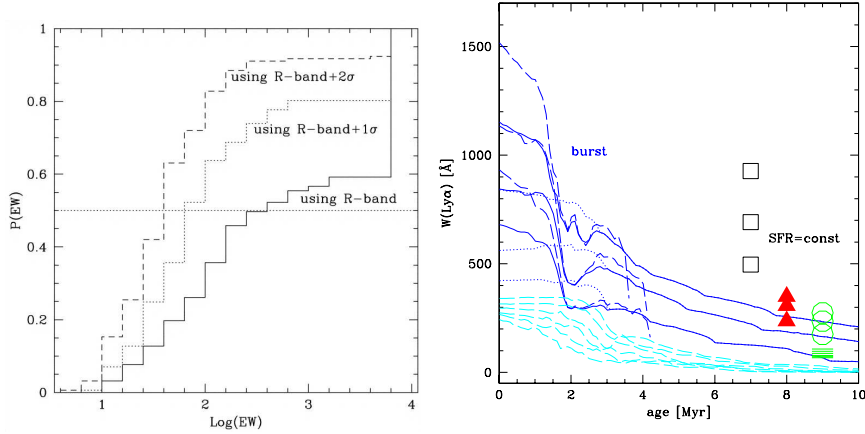


Fig. 1.10. **Left:** Observed Ly $\alpha$  equivalent width distribution of  $z = 4.5$  sources from the LALA survey From Malhotra & Rhoads (2002). **Right:** Predicted Ly $\alpha$  equivalent width for starbursts at different metallicities (from solar to PopIII). Normal metallicities ( $Z \gtrsim 1/50 Z_{\odot}$ ) are shown by the magenta dashed lines. The maximum value predicted in this case is  $W(\text{Ly}\alpha) \sim 300 \text{ \AA}$ . From Schaerer (2003).

achieved depth ( $\text{He II } \lambda 1640/\text{Ly}\alpha < 13\text{--}20 \%$  at  $2\text{--}3 \sigma$  and  $W(\text{He II } \lambda 1640) < 17\text{--}25 \text{ \AA}$ ) may not be sufficient. The origin of these high  $W(\text{Ly}\alpha)$  remains thus unclear.

However, there is some doubt on the reality of the LALA high equivalent widths measured from NB and broad-band imaging, or at least on them being so numerous even at  $z = 4.5$ . First of all the objects with the highest  $W(\text{Ly}\alpha)$  have very large uncertainties since the continuum is faint or non-detected. Second, the determination of  $W(\text{Ly}\alpha)$  from a NB and a centered broad-band filter ( $R$ -band in the case of Malhotra & Rhoads 2002) may be quite uncertain, e.g. due to unknowns in the continuum shape, the presence of a strong spectral break within the broad-band filter etc. (see Hayes & Oestlin 2006 for a quantification, and Shimasaku et al. 2006). Furthermore other groups have not found such high  $W$  objects (Hu et al. 2004, Ajiki et al. 2003) suggesting also that this may be related to insufficient depth of the LALA photometry.

More recently larger samples of LAE were obtained, e.g. at  $z = 5.7$  (e.g. Shimasaku et al. 2006 has 28 spectroscopically confirmed objects). Although their *observed* restframe equivalent widths  $W_{\text{obs}}^{\text{rest}}(\text{Ly}\alpha)$  (median value and  $W$  distribution) are considerably lower than those of



Malhotra & Rhoads at  $z = 4.5$ , and only few objects (1–3 out of 34) show  $W_{\text{obs}}^{\text{rest}}(\text{Ly}\alpha) \gtrsim 200 \text{ \AA}$ , it is possible that in several of these objects the maximum Ly $\alpha$  equivalent width of normal stellar populations is indeed exceeded. This would clearly be the case if the IGM transmission at this redshift is  $T_\alpha \sim 0.3\text{--}0.5$  (cf. Shimasaku et al. 2006, Dijkstra et al. 2006c), which would imply that the true intrinsic  $W^{\text{rest}} = 1/T_\alpha \times W_{\text{obs}}^{\text{rest}}$  is  $\sim 2\text{--}3$  times higher than the observed one. Shimasaku et al. estimate that  $\sim 30\text{--}40\%$  of their LAE have  $W^{\text{rest}}(\text{Ly}\alpha) \geq 240 \text{ \AA}$  and suggest that these may be young galaxies or again objects with PopIII contribution. Dijkstra & Wyithe (2007), based on Ly $\alpha$ -LF and  $W(\text{Ly}\alpha)$  modeling, also argue for the presence of PopIII stars in this  $z = 5.7$  LAE sample.

Another interesting result is the increase of the fraction of large  $W(\text{Ly}\alpha)$  LBGs with redshift, e.g. from  $\sim 2\%$  of the objects with  $W^{\text{rest}}(\text{Ly}\alpha) > 100 \text{ \AA}$  at  $\sim 3$  to  $\sim 80\%$  at redshift 6, which is tentatively attributed lower extinction, younger ages or an IMF change (Shimasaku et al. 2006, Nagao et al. 2007).

Despite these uncertainties it is quite clear that several very strong LAE emitters are found and that these objects are probably the most promising candidates to detect direct *in situ* signatures of PopIII at high redshift (see also Scannapieco et al. 2003). Searches are therefore ongoing (e.g. Nagao et al. 2005) and the first such discovery may be “just around the corner”, or may need more sensitive spectrographs and multi-object near-IR spectroscopy (cf. Sect. 1.4.4).

#### 1.4.2.2 Dust properties of high- $z$ LAE

Although there are indications that LAE selected through their Ly $\alpha$  emission are mostly young and relatively dust free objects (e.g. Shimasaku et al. 2006, Pirzkal et al. 2006, Gawiser et al. 2006), it is of great interest to search for signatures of dust in distant/primeval galaxies †. Furthermore some models predict a fairly rapid production and the presence of significant amounts of dust at high- $z$  (Mao et al. 2006). LAE have the advantage of being at known redshift and of indicating the presence of massive stars. SED fits of such objects must therefore include populations of  $< 10$  Myr age providing thus an additional constraint on modeling.

Recently the stellar populations of some high- $z$  LAEs have been analysed with such objectives in mind. For example the  $z = 6.56$  gravitationally lensed LAE discovered by Hu et al. (2002) has recently been

† Remember that e.g. sub-mm selected galaxies – i.e. very dusty objects – or at least a subsample of them show also Ly $\alpha$  emission (Chapman et al. 2003).

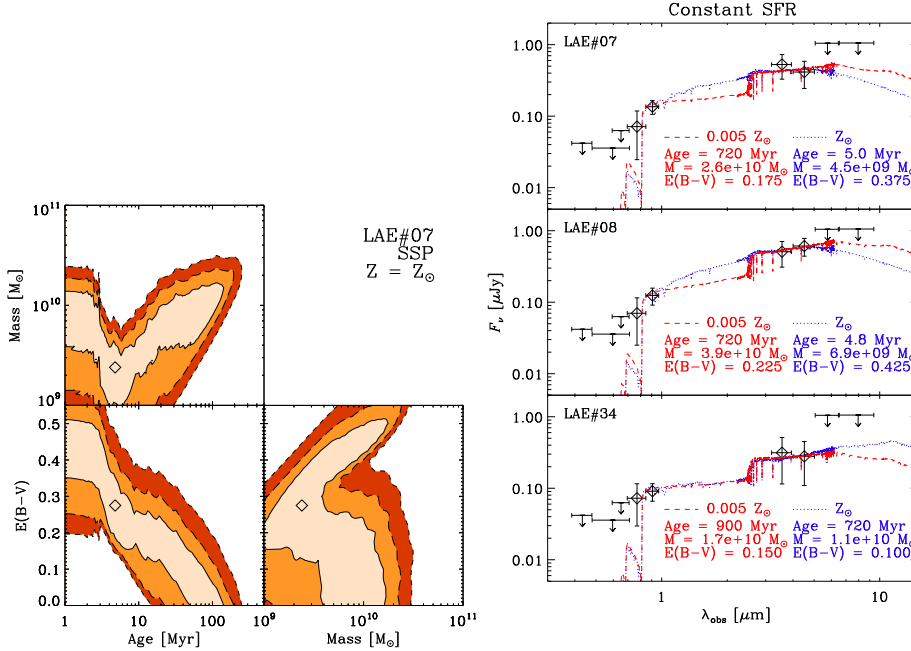


Fig. 1.11. Illustrations of SED fits to  $z = 5.7$  LAE from Lai et al. (2007). **Left:**  $\chi^2$  contour plots showing the best solution for one object and degeneracies in the fit parameter. **Right:** Comparison of best fit SEDs with constant SFR to observations for 3 LAE. These results show indications for the presence of dust in  $z = 5.7$  LAE. See text for discussion.

analysed by Schaerer & Pelló (2005), who find that a non-negligible extinction ( $A_V \sim 1$ ) may be necessary to reconcile the relatively red UV-restframe SED and the presence of Ly $\alpha$ . Later this interpretation was supported by Chary et al. (2005) including also longer wavelength photometry obtained with Spitzer. Three NB selected LAE at  $z = 5.7$  detected in the optical and with Spitzer at 3.6 and 4.5  $\mu m$ , have recently been analysed by Lai et al. (2007). Overall they find SED fits degenerate in age, extinction, metallicity and SF history with stellar population ages up to 700 Myr. Most solutions require some dust extinction (see Fig. 1.11). If the need for Ly $\alpha$  emission, i.e. for the presence of young (massive) stars is taken into account, it seems that a constant SFR scenario is likely together with an extinction of  $E_{B-V} \sim 0.1-0.2$ .

Although still uncertain, these four  $z \sim 5.7-6.6$  galaxies provide currently to my knowledge the best indications for dust in “normal” galaxies

around 1 Gyr after the Big Bang †. As already mentioned, these objects are probably not representative of the typical high- $z$  LAE, but they may be of particular interest for direct searches of high- $z$  dust. In any case, the first attempts undertaken so far to detect dust emission from  $z \sim 6.5$  galaxies in the sub-mm (Webb et al. 2007, Boone et al. 2007) have provided upper limits on their dust masses of the order of  $\sim (2 - 6) \times 10^8 M_{\odot}$ . Future observations with more sensitive instruments and targeting gravitationally lensed objects should soon allow progress in this field.

### 1.4.3 Lyman-break galaxies

In general Lyman-break galaxies (LBGs) are better known than the galaxies selected by Ly $\alpha$  emission (LAE) discussed above. There is a vast literature on LBGs, summarised in an annual review paper in 2002 by Giavalisco (2002). However, progress being so fast in this area, frequent “updates” are necessary. In this last part I shall give an overview of the current knowledge about LBGs at  $z \gtrsim 6$ , trying to present the main methods, results, uncertainties and controversies, and finally to summarise the main open questions. A more general overview about galaxies across the Universe and out to the highest redshift is given in the lectures of Ellis (2007). Recent results from deep surveys including LBGs and LAE can be found in the proceedings from “At the Edge of the Universe” (Afonso et al. 2007). Giavalisco (this Winterschool) also covers in depth galaxy surveys.

The general principle of the LBG selection has already been mentioned above. The number of galaxies identified so far is approximately: 4000  $z \sim 4$  galaxies (B-dropout), 1000  $z \sim 5$  galaxies (V-dropout), and 500  $z \sim 6$  galaxies (i-dropout) according to the largest dataset compiled by Bouwens and collaborators (cf. Bouwens & Illingworth 2006). The number of good candidates at  $z \gtrsim 7$  is still small (cf. below).

#### 1.4.3.1 i-dropout ( $z \sim 6$ ) samples

Typically two different selections are applied to find  $z \sim 6$  objects. 1) a simple  $(i - z)_{AB} > 1.3-1.5$  criterium establishing a spectral break plus optical non-detection, or 2)  $(i - z)_{AB} > 1.3$  plus a blue UV (restframe) slope to select actively star forming galaxies at these redshift. The main samples have been found thanks to deep HST imaging (e.g. in the Hubble Ultra-Deep Field and the GOODS survey), and with SUBARU (see

† Dust emission has been observed in quasars out to  $z \sim 6$ , as discussed briefly in Sect. 1.2.6.

Stanway et al. 2003, 2004, Bunker et al. 2004, Bouwens et al. 2003, Yan et al. 2006)

In general all photometric selections must avoid possible “contamination” by other sources. For the  $i$ -dropouts possible contaminants are: L or T-dwarfs,  $z \sim 1$ –3 extremely red objects (ERO), or spurious detections in the  $z$  band. Deep photometry in several bands (ideally as many as possible!) is required to minimize the contamination. The estimated contamination of  $i$ -drop samples constructed using criterium 1) is somewhat controversial and could reach up to 25 % in GOODS data e.g., according to Bouwens et al. (2006) and Yan et al. (2006). Follow-up spectroscopy has shown quite clearly that L-dwarfs contaminate the bright end of the  $i$ -dropout samples, whereas at fainter magnitudes most objects appear to be truly at high- $z$  (Stanway et al. 2004, Malhotra et al. 2005).

The luminosity function (LF) of  $z \sim 6$  LBGs has been measured and its redshift evolution studied by several groups. Most groups find an unchanged faint-end slope of  $\alpha \sim -1.7$  from  $z \sim 3$  to 6. Bouwens et al. (2006) find a turn-over at the bright end of the LF, which they interpret as being due to hierarchical buildup of galaxies. However, the results on  $M_\star$  and  $\alpha$  remain controversial. For example Sawicki & Thompson (2006) find no change of the bright end of the LF but an evolution of its faint end from  $z \sim 4$  to 2, while other groups (e.g. Bunker et al. 2004, Yoshida et al. 2006, Shimasaku et al. 2006) find similar results as Bouwens et al.. The origin of these discrepancies remain to be clarified.

The luminosity density of LBGs and the corresponding star formation rate density (SFRD) has been determined by many groups up to redshift  $\sim 6$ . Most of the time this is done by integration of the LF down to a certain reference depth, e.g.  $0.3L_\star(z = 3)$ , and at high- $z$  generally no extinction corrections are applied. Towards high- $z$ , the SFRD is found to decrease somewhat from  $z \sim 4$  to 6, whereas beyond this the results are quite controversial as we will discuss (see e.g. a recent update by Hopkins 2006).

The properties of individual galaxies will be discussed in Sect. 1.4.3.3.

#### 1.4.3.2 Optical-dropout samples ( $z \gtrsim 7$ )

Going beyond redshift 7 requires the use of near-IR observations, as the Ly $\alpha$ -break of such objects moves out of the optical window. Given the different characteristics of such detectors and imagers (lower sensitivity and smaller field of view) progress has been less rapid than for lower redshift observations.

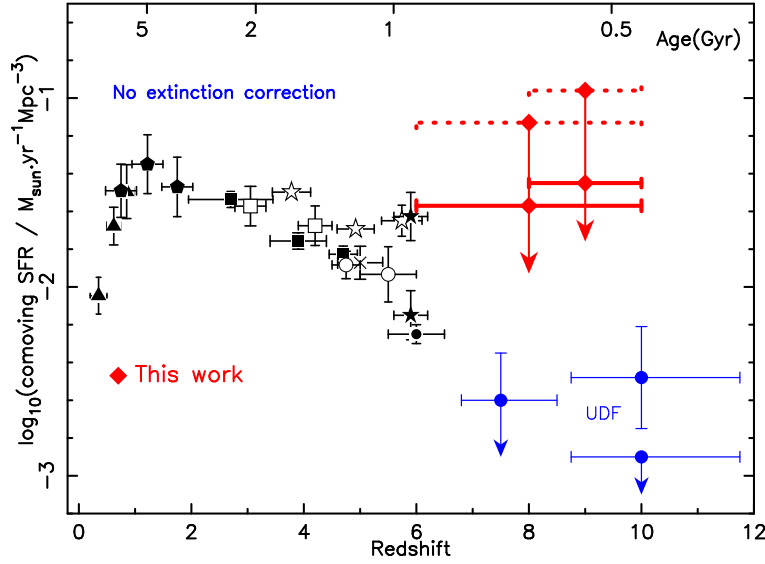


Fig. 1.12. Evolution of the comoving SFR density as a function of redshift including a compilation of results at  $z \lesssim 6$ , estimates from the lensing cluster survey of Richard et al. (2006) for the redshift ranges  $[6 - 10]$  and  $[8 - 10]$ , and the values derived by Bouwens and collaborators from the Hubble Ultra-Deep Field (labeled “UDF”). Red solid lines: SFR density obtained from integrating the LF of the first category candidates of Richard et al. down to  $L_{1500} = 0.3 L_{z=3}^*$ ; red dotted lines: same as red solid lines but including also second category candidates with a detection threshold of  $< 2.5\sigma$  in  $H$ . From Richard et al. (2006).

In the NICMOS Ultra-Deep Field, Bouwens et al. (2004, 2006) have found 1–4  $z$ -dropouts detected in  $J$  and  $K$ , compatible with redshift  $z \sim 7$  starbursts. From this small number of objects and from the non-detection of  $J$ -dropouts by Bouwens et al. (2005) they deduce a low SFR density between  $z \sim 7$  and 10, corresponding to a significant decrease of the SFRD with respect to lower redshift (see Fig. 1.12, symbols labeled “UDF”). The properties of these and other  $z \gtrsim 7$  galaxies will be discussed below.

As an alternative to “blank fields” usually chosen for “classical” deep surveys, the use of gravitational lensing clusters – i.e. galaxy clusters acting as strong gravitational lenses for background sources – has over the last decade or so proven very efficient in finding distant galaxies (e.g. Hu et al. 2002, Kneib et al. 2004). Using this method, and applying the Lyman-break technique plus a selection for blue UV restframe spectra

(i.e. starbursts), our group has undertaken very deep near-IR imaging of several clusters to search for  $z \sim 6$ –10 galaxy candidates (see Schaerer et al. 2006 for an overview). 13 candidates whose SED is compatible with that of star forming galaxies at  $z > 6$  have been found (see Richard et al. 2006 for detailed results). After taking into account the detailed lensing geometry, sample incompleteness, correcting for false-positive detections, and assuming a fixed slope taken from observations at  $z \sim 3$ , their LF was computed. Within the errors the resulting LF is compatible with that of  $z \sim 3$  Lyman break galaxies. At low luminosities it is also compatible with the LF derived by Bouwens et al. (2006) for their sample of  $z \sim 6$  candidates in the Hubble Ultra Deep Field and related fields. However, the turnover observed by these authors towards the bright end relative to the  $z \sim 3$  LF is not observed in the Richard et al. sample. The UV SFR density at  $z \sim 6$ –10 determined from this LF is shown in Fig. 1.12. These values indicate a similar SFR density as between  $z \sim 3$  to 6, in contrast to the drop found from the deep NICMOS fields (Bouwens et al. 2006)<sup>†</sup>. The origin of these differences concerning the LF and SFRD remain unclear until now. In any case, recent follow-up observations with HST and Spitzer undertaken to better constrain the SEDs of the these candidates or to exclude some of them as intermediate- $z$  contaminants, show that the bulk of our candidates are compatible with being truly at high- $z$  (see Schaerer et al. 2007a).

One of the main avenues to clarify these differences is by improving the statistics, in particular by increasing the size (field of view) of the surveys. Both surveys of more lensing clusters and wide blank field near-IR surveys, such as UKIDSS are ongoing. First  $z \sim 7$  candidates have recently been found by UKIDSS (McLure 2007, private communication).

In this context it should also be remembered that not all optical dropout galaxies are at high- $z$ , as a simple “dropout” criterium only relies on a very red color between two adjacent filters. As discussed for the  $i$ -dropouts above, extremely red objects (such as ERO) at  $z \sim 1$ –3 can be selected by such criteria. See Dunlop et al. (2007) and Schaerer et al. (2007b) for such examples. This warning is also of concern for searches for possible massive (evolved) galaxies at high redshift as undertaken by Mobasher et al. (2005) and McLure et al. (2006).

<sup>†</sup> The SFRD values of Bouwens have been revised upwards, reducing the differences with our study (see Hopkins 2007)

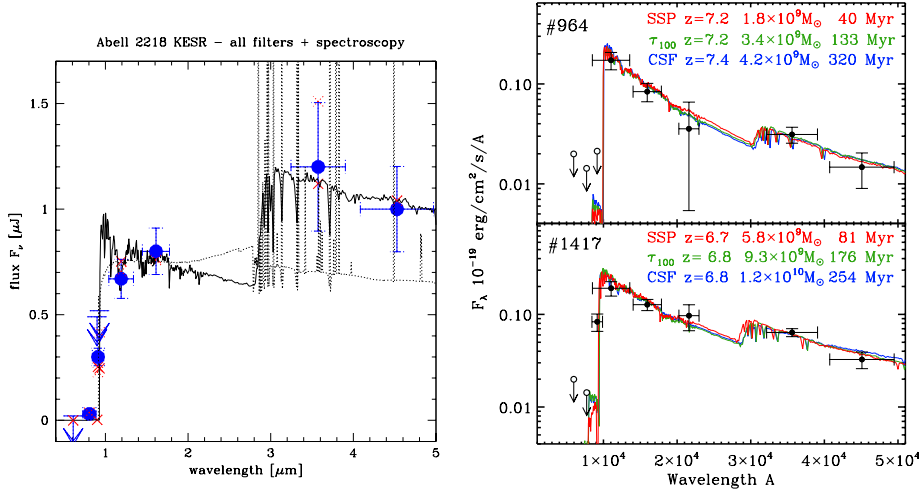


Fig. 1.13. **Left:** Observed SED of the  $z \sim 7$  lensed galaxy from Egami et al. (2005) and model fits from Schaerer & Pelló (2005) showing possible solutions with young ages ( $\sim 15$  Myr, solid line) or with a template of a metal-poor galaxy showing strong emission lines. **Right:** SEDs of two IRAC detected  $z \sim 7$  galaxies from the Hubble Ultra Deep field and best fits using different SF histories. From Labbé et al. (2006). Note the different flux units ( $F_\nu$  versus  $F_\lambda$ ) used in the two plots.

#### 1.4.3.3 Properties of $z \gtrsim 6$ LBG galaxies

Let us now review the main properties of individual  $z \gtrsim 6$  LBG, i.e. continuum selected, galaxies and discuss implications thereof. Ly $\alpha$  emitters (LAE), such as the  $z = 6.56$  lensed galaxy found by Hu et al. (2002), have already been discussed earlier (Sect. 1.4.2). Determinations of stellar populations (ages, SF history), extinction, and related properties of such distant galaxies have really been possible only recently with the advent of the Spitzer space telescope providing sensitive enough imaging at 3.6 and 4.5  $\mu\text{m}$ . These wavelengths, longward of the  $K$ -band and hence not available for sensitive observations from the ground, correspond to the restframe optical domain, which is crucial to constrain properly stellar ages and stellar masses.

A triply lensed galaxy high- $z$  galaxy magnified by a factor  $\sim 25$  by the cluster Abell 2218 has been found by Kneib et al. (2004). Follow-up observations with Spitzer allowed to constrain its SED up to 4.5  $\mu\text{m}$  and show a significant Balmer break (Egami et al. 2005, see Fig. 1.13). Their analysis suggests that this  $z \sim 7$  galaxy is in the poststarburst stage with

an age of at least  $\sim 50$  Myr, possibly a few hundred million years. If true this would indicate that a mature stellar population is already in place at such a high redshift. However, the apparent 4000-Å break can also be reproduced equally well with a template of a young ( $\sim 3 - 5$  Myr) burst, where strong rest-frame optical emission lines enhance the 3.6- and 4.5  $\mu\text{m}$  fluxes (Schaerer & Pelló 2005, and Fig. 1.13). The stellar mass is an order of magnitude smaller ( $\sim 10^9 M_\odot$ ) smaller than that of typical LBG, the extinction low, and its SFR  $\sim 1 M_\odot \text{ yr}^{-1}$ .

Two to four of the four  $z \sim 7$  candidates of Bouwens et al. (2004) discussed above have been detected in the very deep 23.3h exposures taken with Spitzer at 3.6 and 4.5  $\mu\text{m}$  by Labbé et al. (2006). Their SED analysis indicates photometric redshifts in the range 6.7-7.4, stellar masses  $(1 - 10) \times 10^9 M_\odot$ , stellar ages of 50-200 Myr, and star formation rates up to  $\sim 25 M_\odot \text{ yr}^{-1}$ , and low reddening  $A_V < 0.4$ .

Evidence for mature stellar populations at  $z \sim 6$  has also been found by Eyles et al. (2005, 2007). By “mature” or “old” we mean here populations with ages corresponding to a significant fraction of the Hubble time, which is just  $\sim 1$  Gyr at this redshift. Combining HST and Spitzer data from the GOODS survey they find that 40 % of 16 objects with clean photometry have evidence for substantial Balmer/4000- spectral breaks. For these objects, they find ages of  $\sim 200-700$  Myr, implying formation redshifts of  $7 \leq z_f \leq 18$ , and large stellar masses in the range  $\sim (1 - 3) \times 10^{10} M_\odot$ . Inverting the SF histories of these objects they suggest that the past global star formation rate may have been much higher than that observed at the  $z \sim 6$  epoch, as shown in Fig. 1.14. This could support the finding of a relatively high SFR density at  $z \gtrsim 7$ , such as found by Richard et al. (2006).

In short, although the samples of  $z > 6$  Lyman break galaxies for which detailed information is available are still very small, several interesting results concerning their properties emerge already: mature stellar populations in possibly many galaxies indicating a high formation redshift, stellar masses of the order of  $10^9$  to  $10^{10} M_\odot$ , and generally low extinction. However a fraction of these galaxies appears also to be young and less massive (cf. Eyles et al. 2007) forming a different “group”. Similar properties and similar two groups are also found among the high- $z$  LAE (cf. Schaefer & Pelló 2005, Lai et al. 2007, and Pirzkal et al. 2006) already discussed above. Whether such separate “groups” really exist and if so why, or if there is a continuity of properties remains to be seen.

In a recent analysis Verma et al. (2007) find that  $\sim 70$  % of  $z \sim 5$  LBGs have typical ages of  $\lesssim 100$  Myr, and stellar masses of  $\sim 10^9 M_\odot$ , which



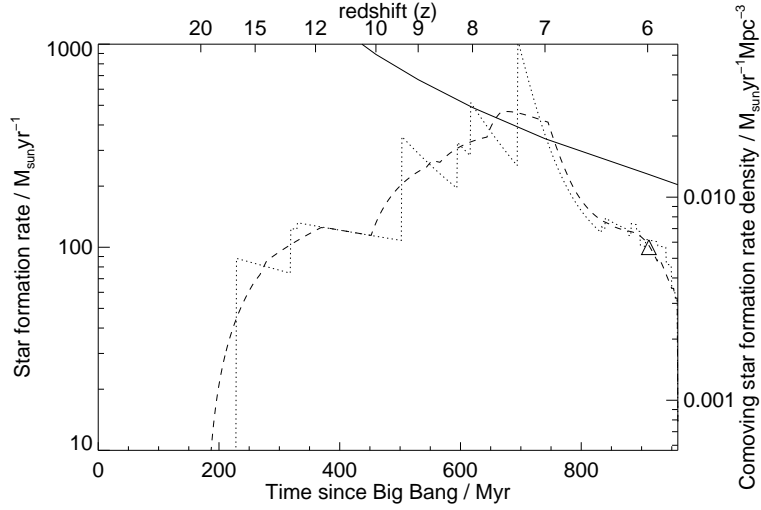


Fig. 1.14. History of the star formation rate density determined by inversion from the observed  $i$ -dropout galaxies analysed by Eyles et al. (2007). The dotted curve is the sum of the past star formation rates for our  $i'$ -drop sample (left axis, with the corresponding star formation rate density shown on the right axis, corrected for incompleteness including a factor of 3.2 for galaxies below the flux threshold). The dashed curve is this star formation history smoothed on a timescale of 100 Myr. The triangle is the estimate of the unobscured (rest-frame UV) star formation rate density at  $z \approx 6$  from  $i'$ -drops in the HUDF from Bunker et al. (2004). The solid curve shows the condition for reionisation from star formation, as a function of time (bottom axis) and redshift (top axis), assuming an escape fraction of unity for the Lyman continuum photons. From Eyles et al. (2007).

are younger and less massive than typical LBGs at  $z \sim 3$ . They also find indications for a relatively low extinction, lower than at  $z \sim 3$ . The trend of a decreasing extinction in LBGs with increasing redshift has been found by many studies, and is in agreement with the results discussed above for  $z \sim 6$  and higher. However, the differences in age and mass e.g. compared with the objects of Eyles et al. (2007) may be surprising, especially given the short time ( $\sim 200$  Myr) between redshift 5 and 6. Several factors, such as selection effects, the representativity of the small  $z \sim 6$  samples studied in detail, etc. may contribute to such differences. Reaching a more complete and coherent understanding of the different primeval galaxy types, of their evolution, and their relation with galaxies at lower redshift will need more time and further observations.

**1.4.4 What next?**

As shown in these lectures it has been possible during the last decade to push the observational limits out to very high redshift and to identify and to study the first samples of galaxies observed barely  $\sim 1$  Gyr after the Big Bang. The current limit is approximately at  $z \sim 7-10$ , where just few galaxies (or galaxy candidates) have been detected, and where spectroscopic confirmation remains extremely challenging.

Thanks to very deep imaging in the near-IR domain it is possible to estimate or constrain the stellar populations (age, SF history, mass, etc.) and dust properties (extinction) of such “primeval” galaxies, providing us with a first glimpse on galaxies in the early universe. Despite this great progress and these exciting results, the global observational picture on primeval galaxies, their formation and evolution, remains to be drawn. Many important questions remain or, better said, start to be posed now, and can now or in the near future be addressed not only by theory and modeling but also observationally!

We have already seen some of the emerging questions in several parts of these lecture. Others, sometimes more general ones, have not been addressed. Among the important questions concerning primeval galaxies we can list:

- How do different high- $z$  populations such as LAE and LBG fit together? Are there other currently unknown populations? What are the evolutionary links between these populations and galaxies at lower redshift?
- What is the metallicity of the high- $z$  galaxies? Where is Population III?
- What is the star formation history of the universe during the first Gyr after Big Bang?
- Are there dusty galaxies at  $z \gtrsim 6$ ? How, where, when, and how much dust is produced at high redshift?
- Which are the sources of reionisation? And, are these currently detectable galaxies or very faint low mass objects? What is the history of cosmic reionisation?

We, and especially you the young students, are fortunate to live in a period where theory, computing power, and many future observational facilities are rapidly growing, enabling astronomers to peer even deeper into the universe. It is probably a fair guess to say that within the next 10-20 years we should have observed the truly first galaxies forming

in the universe, found Population III, etc. We will thus have reached the limits of the map in this exploration of the universe. However, a lot of challenging and interesting work will remain to reach a global and detailed understanding of the formation and evolution of stars and galaxies!

#### ***Acknowledgements***

I thank Jordi Cepa for the invitation to lecture on this topic and for his patience with the manuscript. I would also like to thank him and the IAC team for the organisation of this excellent and enjoyable winterschool. Over the last years I've appreciated many interesting and stimulating discussions with my collaborators and other colleagues. Among them I'd like to thank in particular Roser Pelló, Johan Richard, Jean-François Le Borgne, Jean-Paul Kneib, Angela Hempel, and Eiichi Egami representing the “high”- $z$  universe, Daniel Kunth, Anne Verhamme, Hakim Atek, Matthew Hayes, and Miguel Mas-Hesse for the nearby universe, as well as Andrea Ferrara, Grazyna Stasińska, and David Valls-Gabaud. Both the list of people to thank and the literature list is quite incomplete though. Apologies.

## References

- Afonso, J., Ferguson H., Norris, R., Eds., 2007, “At the Edge of the Universe: latest results from the deepest astronomical surveys”, ASP Conf. Series, in press
- Ahn, S.H., 2004, ApJ, 601, L25
- Ajiki, M., et al., 2003, AJ, 126, 2091
- Baraffe, I., Heger, A., Woosley, S.E., 2001, ApJ, 552, 464
- Barkana, R., Loeb, A., 2001, Physics Reports, 349, 125
- Boone, F., Schaerer, D., et al., 2007, A&A, in preparation
- Bouwens, R. J., et al. 2003, ApJ, 595, 589
- Bouwens, R. J., & Illingworth, G. D. 2006, Nature, 443, 189
- Bouwens, R. J., Illingworth, G. D., Blakeslee, J. P., & Franx, M. 2006, ApJ, 653, 53
- Bouwens, R. J., Illingworth, G. D., Thompson, R. I., & Franx, M. 2005, ApJL, 624, L5
- Bouwens R. J., Thompson R. I., Illingworth G. D., Franx M., van Dokkum P., Fan X., Dickinson M. E., Eisenstein D. J., Rieke M. J., 2004, ApJ, 616, L79
- Bromm & Larson (2004, ARA&A)
- Bromm, V. , Kudritzki, R.P., Loeb, A., 2001, ApJ, 552, 464
- Bunker, A. J., Stanway, E. R., Ellis, R. S., & McMahon, R. G. 2004, MNRAS, 355, 374
- Cen, R., Haiman, Z., 2000, ApJ, 542, L75
- Chapman, S. C., Blain, A. W., Ivison, R. J., & Smail, I. R. 2003, Nature, 422, 695
- Charlot, S., Fall, S. M. 1993, ApJ, 415, 580
- Chary, R.-R., Stern, D., & Eisenhardt, P. 2005, ApJL, 635, L5
- Ciardi, B., & Ferrara, A. 2005, Space Science Reviews, 116, 625
- Ciardi, B., Ferrara, A., Governato, F., & Jenkins, A. 2000, MNRAS, 314, 611
- Dawson, S., et al. 2004, ApJ, 617, 707
- Dijkstra, M., Haiman, Z., & Spaans, M. 2006a, ApJ, 649, 37
- Dijkstra, M., Haiman, Z., & Spaans, M. 2006b, ApJ, 649, 14
- Dijkstra, M., Wyithe, J.S.B., 2007, MNRAS, submitted [astro-ph/0704.1671]
- Dijkstra, M., Wyithe, J.S.B., Haiman, Z., 2006c, MNRAS, submitted [astro-ph/0611195]

- Dopita, M.A., Sutherland, R.S., 2003, “Astrophysics of the Diffuse Universe”, Springer Verlag
- Dunlop, J. S., Cirasuolo, M., & McLure, R. J. 2007, MNRAS, 376, 1054
- Egami, E., et al. 2005, ApJL, 618, L5
- Ekström, S., Meynet, G., & Maeder, A. 2006, Stellar Evolution at Low Metallicity: Mass Loss, Explosions, Cosmology, 353, 141
- Ellis, R.S., 2007, in “First Light in the Universe”, 36th Saas-Fee advanced course, Eds. D. Schaerer, A. Hempel, D. Puy, Springer Verlag, in press [astro-ph/0701024]
- Eyles, L. P., Bunker, A. J., Ellis, R. S., Lacy, M., Stanway, E. R., Stark, D. P., & Chiu, K. 2007, MNRAS, 374, 910
- Eyles, L. P., Bunker, A. J., Stanway, E. R., Lacy, M., Ellis, R. S., & Doherty, M. 2005, MNRAS, 364, 443
- Fan, X., et al. 2003, AJ, 125, 1649
- Fan, X., Carilli, C. L., & Keating, B. 2006, ARAA, 44, 415
- Ferrara, A., 2007, in “First Light in the Universe”, 36th Saas-Fee advanced course, Eds. D. Schaerer, A. Hempel, D. Puy, Springer Verlag, in press [obswww.unige.ch/saas-fee2006/]
- Ferrara, A., & Ricotti, M. 2006, MNRAS, 373, 571
- Finkelstein, S.L., Rhoads, J.E., Malhotra, S., Pirzkal, N., Wang, J., 2006, ApJ, submitted [astro-ph/0612511]
- Furlanetto, S. R., Hernquist, L., & Zaldarriaga, M. 2004, MNRAS, 354, 695
- Furlanetto, S. R., Zaldarriaga, M., & Hernquist, L. 2006, MNRAS, 365, 1012
- Gawiser, E., et al. 2006, ApJL, 642, L13
- Giavalisco, M. 2002, ARAA, 40, 579
- Giavalisco, M., Koratkar, A., & Calzetti, D. 1996, ApJ, 466, 831
- Gnedin, N. Y., & Prada, F. 2004, ApJL, 608, L77
- Haiman, Z., 2002, ApJ, 576, L1
- Haiman, Z., Cen, R., 2005, ApJ, 623, 627
- Haiman, Z., & Spaans, M. 1999, ApJ, 518, 138
- Hansen, M., Oh, S.P., 2006, MNRAS, 367, 979
- Hartmann, L.W., Huchra, J.P., Geller, M.J., 1984, ApJ, 287, 487
- Hayes, M., Östlin, G. 2006, A&A, 460, 681
- Hayes, M., Östlin, G., Mas-Hesse, J. M., Kunth, D., Leitherer, C., & Petrosian, A. 2005, A&A, 438, 71
- Heger, A., & Woosley, S. E. 2002, ApJ, 567, 532
- Heger, A., Fryer, C. L., Woosley, S. E., Langer, N., & Hartmann, D. H. 2003, ApJ, 591, 288
- Hernandez, X., & Ferrara, A. 2001, MNRAS, 324, 484
- Hopkins, A.M., 2006, in “At the Edge of the Universe: latest results from the deepest astronomical surveys”, ASP Conf. Series, in press [astro-ph/0611283]
- Hu, E. M., Cowie, L. L., McMahon, R. G., Capak, P., Iwamuro, F., Kneib, J.-P., Maihara, T., & Motohara, K. 2002, ApJL, 568, L75
- Hu, E. M., Cowie, L. L., Capak, P., McMahon, R. G., Hayashino, T., & Komiyama, Y. 2004, AJ, 127, 563
- Hu, E. M., & Cowie, L. L. 2006, Nature, 440, 1145
- Hu, E. M., Cowie, L. L., Capak, P., & Kakazu, Y. 2005, IAU Colloq. 199: Probing Galaxies through Quasar Absorption Lines, 363 [astro-ph/0509616]
- Hummer, D.G., 1962, MNRAS, 125, 21

- Iye, M., et al. 2006, *Nature*, 443, 186
- Jimenez, R., & Haiman, Z. 2006, *Nature*, 440, 501
- Kashikawa, N., et al. 2006, *ApJ*, 648, 7
- Kneib, J.-P., Ellis, R.S., Santos, M.R., Richard, J., 2004, *ApJ*, 607, 697.
- Kudritzki, R.P., 2002, *ApJ*, 577, 389
- Kunth, D., Leitherer, C., Mas-Hesse, J. M., Östlin, G., & Petrosian, A. 2003, *ApJ*, 597, 263
- Kunth, D., Lequeux, J., Sargent, W. L. W., & Viallefond, F. 1994, *A&A*, 282, 709
- Kunth, D., Mas-Hesse, J. M., Terlevich, E., Terlevich, R., Lequeux, J., & Fall, S. M. 1998, *A&A*, 334, 11
- Labbé, I., Bouwens, R., Illingworth, G. D., & Franx, M. 2006, *ApJL*, 649, L67
- Lai, K., Huang, J.-S., Fazio, G., Cowie, L. L., Hu, E. M., & Kakazu, Y. 2007, *ApJ*, 655, 704
- Le Delliou, M., Lacey, C., Baugh, C. M., Guiderdoni, B., Bacon, R., Courtois, H., Sousbie, T., & Morris, S. L. 2005, *MNRAS*, 357, L11
- Le Delliou, M., Lacey, C. G., Baugh, C. M., & Morris, S. L. 2006, *MNRAS*, 365, 712
- Madau, P. 1995, *ApJ*, 441, 18
- Maiolino, R., Schneider, R., Oliva, E., Bianchi, S., Ferrara, A., Mannucci, F., Pedani, M., & Roca Sogorb, M. 2004, *Nature*, 431, 533
- Malhotra, S., et al. 2005, *ApJ*, 626, 666
- Malhotra, S., Rhoads, J.E., 2002, *ApJ*, 565, L71
- Malhotra, S., & Rhoads, J. E. 2004, *ApJL*, 617, L5
- Mao, J., Lapi, A., Granato, G.L., De Zotti, G., Danese, L., 2006, *ApJ*, submitted [astro-ph/0611799]
- Marigo, P., Girardi, L., Chiosi, C., Wood, R., 2001, *A&A*, 371, 152
- Mas-Hesse, J. M., Kunth, D., Tenorio-Tagle, G., Leitherer, C., Terlevich, R. J., & Terlevich, E. 2003, *ApJ*, 598, 858
- McLure, R. J., et al. 2006, *MNRAS*, 372, 357
- Meier, D., Terlevich, R., 1981, *ApJ*, 246, L109
- Miralda-Escude, J. 1998, *ApJ*, 501, 15
- Meynet, G., Ekström, S., & Maeder, A. 2006, *A&A*, 447, 623
- Nagao, T., Motohara, K., Maiolino, R., Marconi, A., Taniguchi, Y., Aoki, K., Ajiki, M., & Shioya, Y. 2005, *ApJL*, 631, L5
- Nagao, T., et al., 2007, *A&A*, submitted [astro-ph/0702377]
- Neufeld, D.A., 1990, *ApJ*, 350, 216
- Neufeld, D.A., 1991, *ApJ*, 370, 85
- Osterbrock, D.E., Ferland, G.J., 2006, “Astrophysics of Gaseous Nebulae and Active Galactic Nuclei”, 2nd Edition, University Science Books, Sausalito, California
- Ouchi, M. et al., 2005, *ApJ*, 620, L1
- Partridge, R. B., Peebles, J. E. 1967, *ApJ*, 147, 868
- Pelló, R., Schaerer, D., Richard, J., Le Borgne, J.-F., & Kneib, J.-P. 2004, *A&A*, 416, L35
- Pettini, M., Steidel, C. C., Adelberger, K. L., Dickinson, M., & Giavalisco, M. 2000, *ApJ*, 528, 96
- Pirzkal, N., Malhotra, S., Rhoads, J.E., Xu, C., 2006, *ApJ*, submitted [astro-ph/0612513]
- Pritchett, J.C., 1994, *PASP*, 106, 1052

- Richard, J., Pelló, R., Schaerer, D., Le Borgne, J.-F., & Kneib, J.-P. 2006, *A&A*, 456, 861
- Santos, M.R., 2004, *MNRAS*, 349, 1137
- Sawicki, M., & Thompson, D. 2006, *ApJ*, 642, 653
- Schaerer, D. 2002, *A&A*, 382, 28.
- Schaerer, D. 2003, *A&A*, 397, 527.
- Schaerer, D., Hempel, A., Egami, E., Pelló, R., Richard, J., Le Borgne, J.-F., Kneib, J.-P., Wise, M., Boone, F., 2007b, *A&A*, in press [astro-ph/0703387]
- Schaerer, D., Pelló, R., 2005, *MNRAS*, 362, 1054
- Schaerer, D., Pelló, R., Richard, J., Egami, E., Hempel, A., Le Borgne, J.-F., Kneib, J.-P., Wise, M., Boone, F., Combes, F., 2006, *The Messenger*, 125, 20
- Schaerer, D., Pelló, R., Richard, J., Egami, E., Hempel, A., Le Borgne, J.-F., Kneib, J.-P., Wise, M., Boone, F., Combes, F., 2007a, in “At the Edge of the Universe: latest results from the deepest astronomical surveys”, *ASP Conf. Series*, in press [astro-ph/0701195]
- Scannapieco, E., Madau, P., Woosley, S., Heger, A., & Ferrara, A. 2005, *ApJ*, 633, 1031
- Scannapieco, E., Schneider, R., & Ferrara, A. 2003, *ApJ*, 589, 35
- Schneider, R., Ferrara, A., Natarajan, P. & Omukai, K., 2002, *ApJ*, 579, 30
- Schneider, R., Ferrara, A., & Salvaterra, R. 2004, *MNRAS*, 351, 1379
- Schneider, R., Salvaterra, R., Ferrara, A., & Ciardi, B. 2006, *MNRAS*, 369, 825
- Shapiro, P. R., & Giroux, M. L. 1987, *ApJL*, 321, L107
- Shapley, A., Steidel, C. C., Pettini, M., Adelberger, K. L. 2003, *ApJ*, 588, 65
- Shimasaku, K., et al. 2006, *PASJ*, 58, 313
- Spitzer, L., 1978, “Physical Processes in the Interstellar Medium”, Wiley, New York
- Stanway, E. R., Bunker, A. J., & McMahon, R. G. 2003, *MNRAS*, 342, 439
- Stanway, E. R., Bunker, A. J., McMahon, R. G., Ellis, R. S., Treu, T., & McCarthy, P. J. 2004, *ApJ*, 607, 704
- Stark, D.P., Ellis, R.S., Richard, J., Kneib, J.-P., Smith, G.P., Santos, M.R., 2007, *ApJ*, submitted [astro-ph/0701279]
- Steidel, C. C., Giavalisco, M., Dickinson, M., & Adelberger, K. L. 1996, *AJ*, 112, 352
- Stern, D., & Spinrad, H. 1999, *PASP*, 111, 1475
- Stratta, G., et al., 2007, *ApJ*, submitted [astro-ph/0703349]
- Taniguchi, Y., et al. 2005, *PASJ*, 57, 165
- Tapken, C., Appenzeller, I., Noll, S., Richling, S., Heidt, J., Meinkoehn, E., & Mehlert, D. 2007, *A&A*, in press [astro-ph/0702414]
- Tegmark, M., Silk, J., Rees, M. J., Blanchard, A., Abel, T., & Palla, F. 1997, *ApJ*, 474, 1
- Tenorio-Tagle, G., Silich, S.A., Kunth, D. et al. 1999, *MNRAS*, 309, 332
- Thuan, T. X., & Izotov, Y. I. 1997, *ApJ*, 489, 623
- Thuan, T. X., Sauvage, M., & Madden, S. 1999, *ApJ*, 516, 783
- Todini, P., & Ferrara, A. 2001, *MNRAS*, 325, 726
- Tumlinson, J., Giroux, M.L., Shull, J.M., 2001, *ApJ*, 550, L1
- Tumlinson, J. 2006, *ApJ*, 641, 1
- Valls-Gabaud, D. 1993, *ApJ*, 419, 7
- Verhamme, A., Schaerer, D., & Maselli, A. 2006, *A&A*, 460, 397

- Verhamme, A., Schaerer, D., Atek, H., Tapken, C., 2007, A&A, in preparation
- Verma, A., Lehnert, M.D., Förster Schreiber, N.M., Bremer, M.N., Douglas, L., 2007, MNRAS, in press [astro-ph/0701725]
- Walter, F., et al. 2003, Nature, 424, 406
- Wang, J. X., et al. 2004, ApJL, 608, L21
- Webb, T. M. A., Tran, K.-V. H., Lilly, S. J., & van der Werf, P. 2007, ApJ, 659, 76
- Weinmann, S. M., & Lilly, S. J. 2005, ApJ, 624, 526
- Wilman, R. J., Gerssen, J., Bower, R. G., Morris, S. L., Bacon, R., de Zeeuw, P. T., & Davies, R. L. 2005, Nature, 436, 227
- Williams, R. E., et al. 1996, AJ, 112, 1335
- Wise, J. H., & Abel, T. 2005, ApJ, 629, 615
- Wu, Y., et al., ApJ, in press [astro-ph/0703283]
- Wyithe, J. S. B., & Loeb, A. 2004, Nature, 432, 194
- Yan, H., Dickinson, M., Giavalisco, M., Stern, D., Eisenhardt, P. R. M., & Ferguson, H. C. 2006, ApJ, 651, 24
- Yoshida, M., et al. 2006, ApJ, 653, 988